GEOLOGIC NOZZLES

Susan Werner Kieffer
U. S. Geological Survey
Flagstaff, Arizona

Abstract. Sonic velocities of geologic fluids, such as volcanic magmas and geothermal fluids, can be as low as 1 m/s. Critical velocities in large rivers can be of the order of 1–10 m/s. Because velocities of fluids moving in these settings can exceed these characteristic velocities, sonic and supersonic gas flow and critical and supercritical shallow-water flow can occur. The importance of the low characteristic velocities of geologic fluids has not been widely recognized, and as a result, the importance of supercritical and supersonic flow in geological processes has generally been underestimated. The lateral blast at Mount St. Helens, Washington, propelled a gas heavily laden with dust into the atmosphere. Because of the low sound speed in this gas (about 100 m/s), the flow was internally supersonic. Old Faithful Geyser, Wyoming, is a converging-diverging nozzle in which liquid water refilling the conduit during the recharge cycle changes during eruption into a two-phase liquid-vapor mixture with a very low sound velocity. The high sound speed of liquid water determines the characteristics of harmonic tremor observed at the gyeser during the recharge interval, whereas the low sound speed of the liquid-vapor mixture influences the fluid flow characteristics of the eruption. At the rapids of the Colorado River in the Grand Canyon, Arizona, the channel is constricted into the shape of a converging-diverging nozzle by debris flows that enter from tributary canyons. Both subcritical and supercritical flow occur within the rapids. The transport capacity in the rapids can be so great that the river contours the channel to a characteristic shape. This shape can be used to interpret the flood history of the Colorado River over the past 10^3–10^5 years. The unity of fluid mechanics in these three natural phenomena is provided by the well-known analogy between gas flow and shallow-water flow in converging-diverging nozzles.

1. INTRODUCTION

This paper was written for the symposium "Perspectives in Fluid Mechanics" held at the California Institute of Technology, January 10–12, 1985. It is specifically an essay of the author's perspective on geologic fluid flow problems, rather than an exhaustive review. For the sake of brevity, references in this paper are limited. The author has published detailed analyses of the three geologic problems presented, and the reader will find references to other relevant work in the cited papers.

2. GEOLOGIC NOZZLES

An eruption of Old Faithful geyser, a flood on the Colorado River, and a lateral blast from Mount St. Helens do not, at first glance, appear to be related. A geographic map of the locations of these three places certainly does not reveal any underlying geologic unity (Figure 1). However, a fluid-dynamical unity is revealed when the "locations" are shown instead on schematic diagrams of gas flowing through a nozzle or of shallow water flowing through a flume (Figure 2) (for example, see *Liepmann and Roshko* [1957, p. 127]). The analogy between the flow fields for compressible gas and shallow water was apparently first described by *Riabouchinsky* [1932] (a more recent and accessible reference is *Loh* [1969, pp. 1–60]). The analogy is semiquantitative and was thus widely explored in the early days of wind tunnel development. In modern times the analogy has been primarily a teaching tool [e.g., *Thompson*, 1972, pp. 517–531] and has never been used by geologists to explain large-scale natural phenomena. The purpose of this paper is to show the basis for invoking nozzle-flow theory for interpretation of complex geologic events and to provide a perspective on geologic problems in which the importance of supercritical and supersonic flow has been underestimated.

A major reason that geologic events have not been viewed from the particular perspective of fluid mechanics presented here is the subdivision of fluid mechanics and its applied fields into the specialties of compressible and incompressible flow, for example, aeronautics versus hydraulics. This subdivision arises from the need to simplify the complex momentum and continuity equations in order to solve most practical problems. In vector form, the momentum equation for a viscous fluid moving in a gravitational field under the influence of a pressure gradient is complex because of dimensionality and nonlinearity:

$$\rho \frac{D\mathbf{u}}{Dt} = -\nabla P + [\nabla \cdot \tau] + \rho \mathbf{g} \qquad (1)$$

Reviews of Geophysics, 27, 1 / *February 1989*
pages 3-38
Paper number 89RG00093

where ρ is the fluid density, D/Dt is the material derivative, $\mathbf{u}$ is the fluid velocity, ∇P is the pressure force acting on the fluid, $\nabla \cdot \tau$ is the viscous force, and $\mathbf{g}$ is the acceleration of gravity. The continuity equation for mass is generally simpler but is still difficult to apply in a geometrically complicated problem:

$$\frac{D\rho}{Dt} = -\rho(\nabla \cdot \mathbf{u}) \tag{2}$$

where $(\nabla \cdot \mathbf{u})$ is the divergence of velocity.

In many cases these two important equations can be considerably simplified by consideration of the fluid properties or the boundary conditions of the problem. For example, if pressure changes are relatively small, compressibility can be neglected so that $\rho \sim$ const and $\nabla \cdot \mathbf{u} = 0$. Such an assumption underlies all of hydraulics, and geologists with interests in hydraulics or related geomorphic problems typically diverge at an early stage of their education from advanced studies of compressible fluid dynamics.

Alternatively, in many flows the pressure gradient may be great enough that compressibility is important but gravity is not; $\mathbf{g} \sim 0$. This latter condition is assumed in most of gas dynamics, and because of the prominent role of gravity in most geologic processes, few geologists are exposed to a rigorous gas dynamics curriculum.

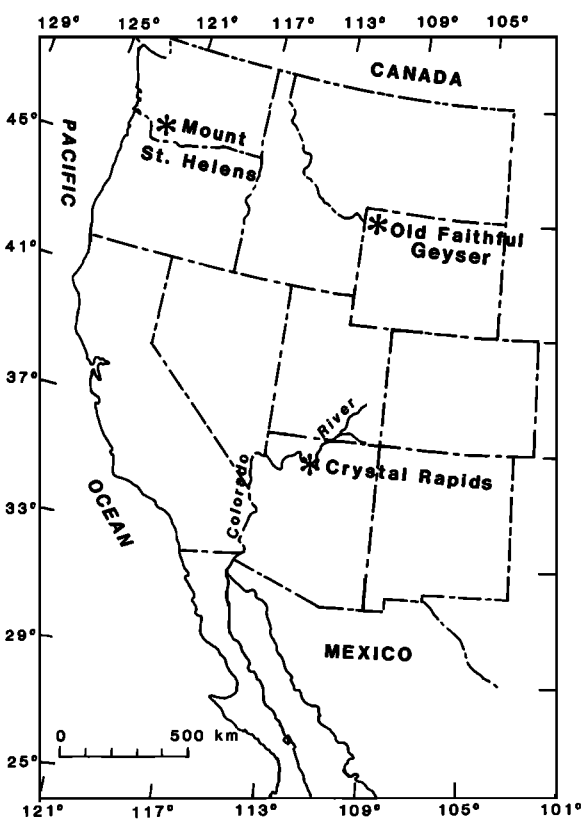

Figure 1. Index map of the geographic locations of Crystal Rapids (Grand Canyon, Arizona), Old Faithful Geyser (Yellowstone National Park, Wyoming), and Mount St. Helens (Washington).

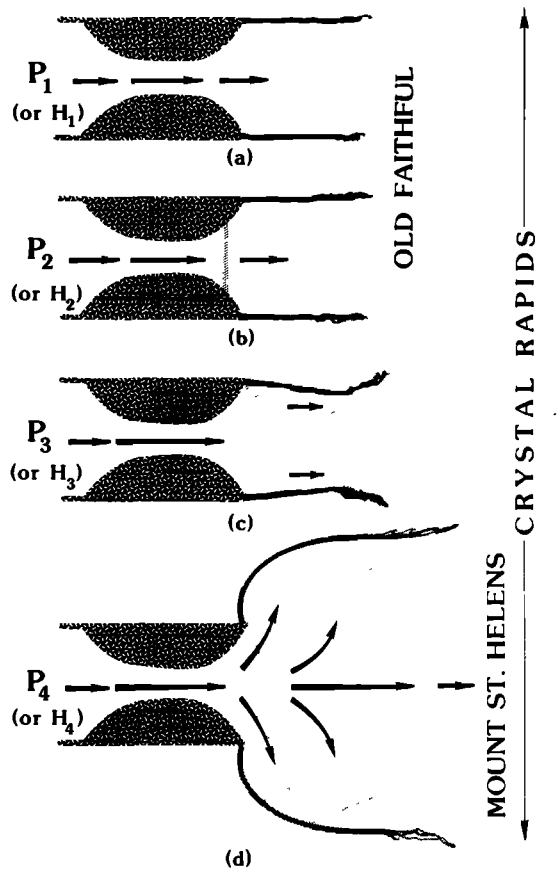

Figure 2. Four diagrams of behavior of gas flowing through a converging-diverging flume. Vector velocities are indicated by arrows. At the exit of the nozzle (or channel), on the right, the structure of the flow field in the departing fluid is shown schematically by the medium shading. Shock and rarefaction waves (alternatively, positive and negative normal and oblique hydraulic jumps) are indicated by the lightest shading.

Although the subjects of nozzle gas dynamics and of shallow-water hydraulics evolve from very different approximations to the conservation equations, important concepts common to both subjects have been recognized because, when reduced to suitable nondimensional variables, the conservation equations in the two subjects become identical. (Readers familiar with this identity can skip directly to the last paragraph of this section and to section 3.)

Examine first the mass and momentum equations for a perfect gas. For simplicity, assume that the flow is quasi-one-dimensional along a coordinate direction x. The equations of mass and momentum conservation for flow of a compressible gas are

$$\frac{\partial \rho}{\partial t} + u\frac{\partial \rho}{\partial x} + \rho\frac{\partial u}{\partial x} = 0 \tag{3}$$

$$\frac{\partial u}{\partial t} + u\frac{\partial u}{\partial x} + \frac{1}{\rho}\frac{\partial P}{\partial x} = 0 \tag{4}$$

For a perfect gas and isentropic flow,

$$PV = RT \tag{5}$$

$$P V^{\gamma} = P_0 V_0^{\gamma} = \text{const} \tag{6}$$

where P is pressure, V is volume, R is the gas constant, T is temperature, and γ is the ratio of specific heats (the isentropic exponent). The subscript zero indicates a reference state (typically one where the fluid is at rest with velocity $u = u_0 = 0$). For a perfect gas, (3)–(6) can be combined to give

$$\frac{\partial u}{\partial t} + u\frac{\partial u}{\partial x} + \frac{\gamma P_0}{\rho_0^{\gamma}}\rho^{\gamma-2}\frac{\partial \rho}{\partial x} = 0 \tag{7}$$

For water flowing from one infinite reservoir into another with lower head, the equations of motion that can be directly compared with (3) and (7) are

$$\frac{\partial h}{\partial t} + u\frac{\partial h}{\partial x} + h\frac{\partial u}{\partial x} = 0 \tag{8}$$

$$\frac{\partial u}{\partial t} + u\frac{\partial u}{\partial x} + g\frac{\partial h}{\partial x} = 0 \tag{9}$$

where h is the water depth. In these equations, and in the figures in this paper, it is assumed that in a vertical cross section (specified by the coordinate z) the bottom of the water is at the channel boundary $z = 0$ and the water has a free surface at $z = h$. The free surface is assumed to be at constant atmospheric pressure P_a, but its elevation can vary along the channel and with time. The velocity of the water can also vary with position along the channel but is assumed constant over any vertical cross section. The viscosity and compressibility of the water are ignored. Again, as with gas flow, quasi-one-dimensional flow is assumed: the contours of the channel walls must be gradual, and vertical accelerations of the water must be small compared with the acceleration of gravity, g.

The shallow-water conservation equations, (8) and (9), are identical to the compressible-gas conservation equations, (3) and (7), if water depth h is analogous to gas density ρ and if the isentropic exponent γ of the gas is equal to 2. Unfortunately, no real gas has such a high value of γ (the highest value being 5/3 for monatomic gases), so that the mathematically equivalent flow fields cannot be quantitatively realized. However, the effect of γ on most flow properties is small, so that the analogy is qualitatively, and even semiquantitatively, useful—as evidenced by the fact that in the early days of rocket design, hydraulic flumes were used to simulate wind tunnels. Examination of the conservation equations and the equations of state for a perfect gas shows that h is also analogous to T and that h^2 is analogous to P. Hence, within the context of all of the simplifying assumptions, flow of gas in a nozzle and flow of shallow water in a flume are governed by the same conservation equations. Identical flow fields therefore occur when the proper nondimensional variables are considered.

The illustrations in Figure 2 represent the flow conditions at different ratios of upstream (reservoir) and downstream (atmosphere or tailwater) conditions. If the figure is interpreted as representing a cross section of a horizontal nozzle through which gas is flowing from left to right, the different parts of the figure represent the flow field from different pressures (P_1, P_2,$\cdots$) in the left reservoirs to lower pressures in the right reservoirs. The low-pressure reservoirs are assumed to be infinitely large and are therefore not shown to scale.

Alternatively, if Figure 2 is interpreted as representing a map view of a horizontal channel in which shallow water is flowing from left to right, the different parts of the figure represent the flow field from reservoirs of different depth. The driving energy for the flow is the elevated depth of water in the left reservoir compared with the right. The water has a potential energy H_r (called the head and generally expressed as a depth), indicated as H_1, H_2 ,$\cdots$, in the parts of Figure 2.

With this introduction, let us reexamine the sense in which each of the geologic problems mentioned above is a nozzle problem. In the spirit of emphasizing the similarity of the various flow fields discussed in this paper, the word "nozzle" will be used interchangeably with the words "flume," "channel," and "conduit," and the word "contouring" will be used interchangeably with the word "eroding." The nozzle of the Colorado River is the river channel, a converging-diverging nozzle formed by debris flows that constrict the main channel, and the fluid is shallow water. The "geologic twist" that complicates simple application of flume concepts is that the walls and bed of the channel are erodible, and the channel can therefore change shape in response to changing conditions in the flow. The nozzle of Old Faithful geyser is a fissure of irregular (and largely unknown) geometry extending more than 20 m into the ground. The geologic twist in this problem is that the fluid is much more complex than a perfect gas: hot, liquid water stands in the conduit between eruptions and then boils and changes through a complex unloading process into a droplet-laden steamy aerosol during an eruption. The nozzle of the Mount St. Helens lateral blast was a huge vent created when a landslide caused by an earthquake opened a vertical scarp nearly 0.25 km^2 in area and exposed a hot hydrothermal and/or magmatic system. The erupting fluid was a hot vapor heavily laden with ash, rocks, ice fragments, and tree debris. As these three examples show, the scale of the geologic nozzles is large, the nozzle shapes are irregular, and the thermodynamic properties of the flowing fluids are complex.

3. SOUND VELOCITIES AND CRITICAL VELOCITIES: THEIR INFLUENCE ON THE FLOW FIELD

The most important result from the above analogy is the recognition that characteristic velocities control flow behavior in shallow water and gas flow. For small disturbances the equations of momentum ((7) and (9)) can be linearized and written as

Perfect gas

$$\frac{\partial^2 P}{\partial t^2} - a_0^2 \frac{\partial^2 P}{\partial x^2} = 0 \tag{10}$$

Shallow water

$$\frac{\partial^2 h}{\partial t^2} - g h_0 \frac{\partial^2 h}{\partial x^2} = 0 \tag{11}$$

These are the well-known wave equations, from which it can immediately be seen that small disturbances propagate with characteristic velocities proportional to the square root of the coefficient of the second term. In compressible gas flow the characteristic velocity is the sound velocity a, the velocity at which small perturbations in density or pressure propagate through the fluid:

$$a^2 = \left(\frac{\partial P}{\partial \rho}\right)_S \tag{12}$$

where the derivative is taken at constant entropy S. In shallow-water flow the characteristic speed is the critical velocity, that is, the velocity of a gravity wave of long wavelength and infinitesmal strength:

$$c^2 = gh \tag{13}$$

In both cases the nature of the flow field depends on the magnitude of the fluid velocity compared with the characteristic velocity. The Mach number M of a compressible gas flow is the ratio of the mean flow velocity to the sound speed:

$$M = u/a \tag{14}$$

The Froude number of shallow-water flow, Fr, is the ratio of the mean flow velocity to the critical velocity:

$$Fr = u/c \tag{15}$$

The local flow variables are determined by these dimensionaless ratios which, in turn, depend on reservoir conditions and geometry. For gas flow the important parameters are the ratio of the pressures in the driving and receiving reservoirs, the area ratio along the axis, and the gas equations of state (particularly R and γ for a perfect gas). For shallow-water flow the important parameters are the ratio of upstream to downstream energy and the area ratio of the channel. Depending on the values of these parameters, the flow field can have dramatically different properties, as illustrated in Figure 2.

Consider, first, that Figure 2 represents the flow of gas through a nozzle. When the pressure P_1 in the reservoir is "low," the fluid accelerates from the reservoir into the constriction and decelerates in the diverging section (Figure 2*a*). This is the classic venturi tube, and the flow is everywhere subsonic. In this context a "low" pressure ratio means that the upstream reservoir pressure is less than about 2 times the downstream reservoir pressure (for example, see the tables of isentropic flow variables given by *Zucrow and Hoffman* [1976]).

If the pressure ratio is higher (Figure 2*b*), the fluid accelerates from the reservoir into the converging section and can reach sonic (choked) conditions (M = 1) in the throat; it can be rigorously shown that sonic conditions can occur only in the throat (for example, see *Zucrow and Hoffman* [1976, p. 166]). At one particular pressure ratio the flow can decelerate back to subsonic conditions in the diverging section, but for higher values it will accelerate to supersonic conditions in the diverging section. Strong nonlinear waves (shock and rarefaction waves) can be present and are, in fact, usually required to decelerate the flow back to ambient conditions in the exit reservoir. At higher pressure ratios for which supersonic flow conditions are obtained, a so-called "normal shock" stands in the diverging section, and the deceleration to ambient conditions occurs within the nozzle through the shock and to the exit plane (Figure 2*b*). At still higher pressure ratios (Figures 2*c* and 2*d*) the shock is "blown out" of the nozzle, and a complicated flow field consisting of oblique and normal shocks and mixed regions of subsonic and supersonic flow exists within the exiting jet. Because the decelerating waves are nonlinear, the jet "overshoots" ambient conditions, and multiple shock and rarefaction waves are required to achieve the pressure balance.

Consider alternatively that Figure 2 represents shallow-water flow. When the head difference between the reservoirs on the left and right is "small," the flow is subcritical everywhere: the fluid accelerates in the converging section and through the constriction, and decelerates in the diverging section (Figure 2*a*). The flow field is analogous to that in a venturi tube. The word "streaming" is often used for subcritical flow. In this context a "small" head difference means that the elevation difference between the upstream and downstream reservoirs should not exceed approximately one third of the head of the source reservoir.

If the head ratio is greater, as indicated in Figure 2*b*, the flow accelerates from the reservoir through the converging section and can reach critical (Fr = 1) conditions in the constriction. At the critical value of head ratio the flow can decelerate to subcritical conditions in the diverging section, but for other higher values it will

accelerate to supercritical conditions in the diverging section. The word "shooting" is often used for supercritical flow. Strong nonlinear waves, in this case called oblique (or slanting) and normal hydraulic jumps, are generally required to decelerate the flow back to ambient conditions in the downstream reservoir. Depending on the head ratio and the severity of the constriction, waves can stand in (Figure 2*b*) or downstream of (Figures 2*c* and 2*d*) the diverging section.

The flow fields shown in Figure 2 are a subset of possible flow conditions, for they do not show possible wave structures that arise if fluid enters the constricted part of the nozzle in a supersonic or supercritical state. Although such conditions can, in fact, be obtained geologically, this complexity is ignored in this paper because the concepts can be extrapolated from the simpler analyses presented here.

Supersonic or supercritical conditions are amazingly easy to obtain in geologic settings. If the ratio of reservoir pressure to atmospheric pressure in a gas nozzle is more than about 2, sonic and supersonic flow will occur in the nozzle; for comparison, the ratio of pressure in a volcanic reservoir to atmospheric pressure is often around 100:1. If shallow water flows from one reservoir to another that has less than two thirds of the head of the source reservoir, critical conditions can be obtained in the throat; for comparison, backwater depths on the Colorado River may exceed downstream tailwater depths by a factor of 2.

Our intuition, however, generally fails to prepare us for the possibility of such flows in the natural world. We commonly think of supersonic flow in terms of modern aeronautics: objects obtain high Mach numbers by moving very fast through air, which has a high sound speed. Geologic fluids rarely move at the speeds characteristic of modern aircraft (except in some volcanic eruptions), but the entire spectrum of flow behavior from subsonic to supersonic (and subcritical to supercritical) can occur in geologic flows because the fluids can have very low characteristic velocities. Fluids with low sound velocities can develop internally supersonic flow fields while still moving subsonically with respect to the surrounding atmosphere. That is, there can be standing shock or rarefication waves internal to the flow but no standing waves in the external medium.

Fluids in geothermal and volcanic settings typically have low sound speeds: water that contains gas or steam bubbles has a very low sound speed, because the bubbles dramatically increase the compressibility of the mixture (κ_S). An alternative form of the definition of sound speed, $a = (1/\kappa_S\rho)^{1/2}$, shows this dependence clearly. The sound speed in an air-water mixture can be as low as 20 m/s. The sound speed is further decreased in a mixture in which the bubbles are of the same composition as the liquid (e.g., steam bubbles in boiling water), because exchanges of mass and latent heat accompany passage of a sound wave; these exchange processes also decrease the sound velocity. Sound speeds as low as 1 m/s are possible for boiling water (reviewed by *Kieffer* [1977]).

The dependence of sound speed on phase, pressure, and temperature can be shown on an entropy-density (S-ρ) phase diagram, in this case for H_2O (Figure 3) (more extensive discussion of this diagram and a similar diagram for CO_2 is given by *Kieffer and Delany* [1979]). This representation is suggested by the definition of sound speed given in (12): on a graph of density versus entropy, sound speed is inversely proportional to the vertical gradient of isobars. Such a graph can be read as an ordinary topographic map (shown schematically in the inset of Figure 3) in which the steepness of the topography is inversely proportional to the spacing of the contours. The S-ρ representation, with its widely spaced isobars in the two-phase region and the steep gradients in the one-phase region, graphically illustrates the wide range of sound speeds characteristic of simple one-component substances.

If volatile fluids like water flow from high to low pressure (e.g., in eruptions or in geothermal wells), the phase of the fluid can change from liquid to liquid plus vapor, or from vapor to vapor plus liquid. A hypothetical decompression path appropriate to Old Faithful (and discussed later in section 5) is shown as the vertical line (a) in Figure 3. Note that along this decompression path the sound speed can change by several orders of magnitude. If the fluid is in a two-phase state, flow velocities of only a few tens of meters per second can give a wide range of Mach numbers, including sonic ($M = 1$) and supersonic ($M > 1$) flow.

Mass loading of vapor with solid fragments or liquid droplets also produces fluids with low sound speeds. No data or theories exist for the fluids encountered in volcanic problems, where, for example, the mass ratio of solids to vapor can exceed 100 and where particle sizes within a single flow can range from microns to meters. At present, we can only apply a simple theory in which the mass-loaded gas is mimicked by perfect gas laws (the so-called "pseudogas" theory) to obtain characteristic sound speeds (Figure 4). Sound speeds of 50–100 m/s are plausible. Flow velocities in gassy volcanic eruptions are commonly of the order of 100 m/s and can exceed 500 m/s. Therefore a wide range of Mach numbers, including $M > 1$, can be obtained.

Finally, note that the critical velocity in shallow-water flow plays the same role as the sound speed in determining transitions between linear and nonlinear flow regimes. Critical velocities in rivers can be of the order of the flow velocities, even in major rivers where large depths increase the critical velocity (equation (13)). In the Colorado River in the Grand Canyon, for example, water depths of the

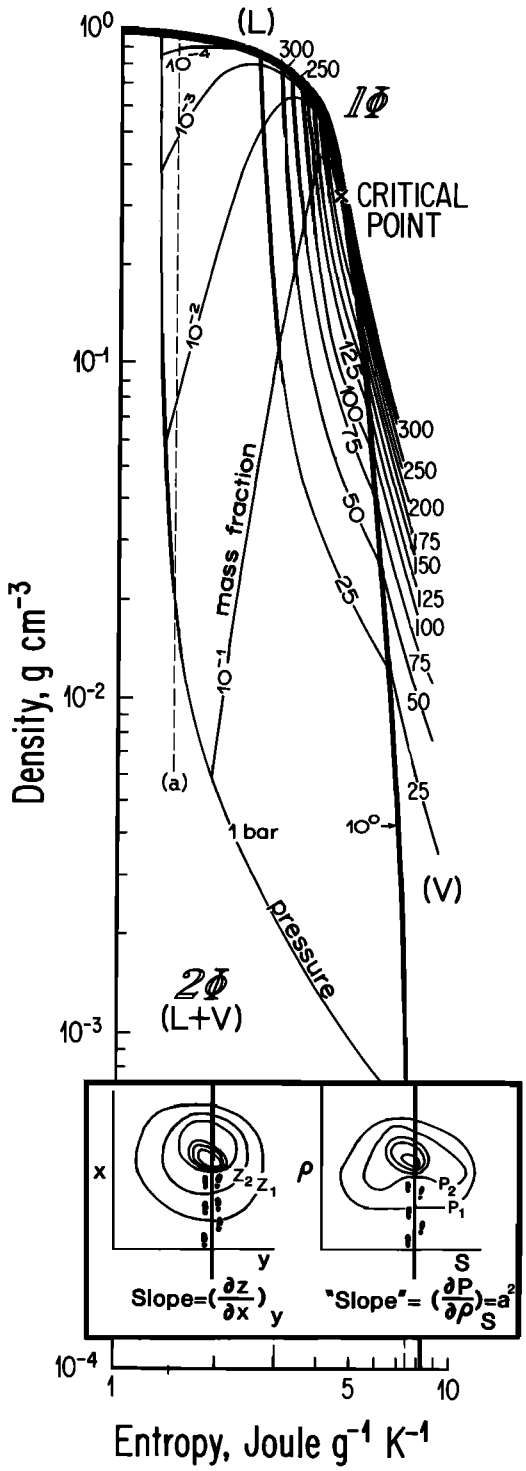

Figure 3. Enropy-density (S-ρ) phase diagram for H_2O (details are given by *Kieffer and Delany* [1979]). Entropy is relative to the triple point of H_2O. The label 1Φ marks the single-phase field, and the label 2Φ marks the two-phase field (L, liquid; V, vapor). Contours of constant pressure (isobars) are shown in 25-bar increments. In the two-phase field, contours of constant mass fraction of vapor (isopleths) are shown. The inset is a comparison of a standard topographic map of a conical hill (left) with the S-ρ diagram (right). The "footsteps" indicate that the appropriate directional derivative to be examined in each case is in the vertical direction.

order of 10 m are common; the corresponding critical velocity is 10 m/s. In most calm stretches of the river, flow velocities are of the order of 1 m/s, and Froude numbers are less than 0.1. In major rapids, however, where the water becomes shallow and fast, the flow velocity can exceed the critical velocity ($Fr > 1$). Supercritical flow is not common in rivers [*Richards*, 1983, p. 58], but when it does occur, the geologic consequences can be great; the situation in the Colorado River, discussed in the following section, is one such occurrence.

Many simplifications have been made in the foregoing discussion, and these, as well as others, will be used in the analyses to follow, e.g., thermodynamic equilibrium; isentropic, quasi-one-dimensional flow; steady flow; and perfect gas or pseudogas behavior. One additional major simplification in the following analyses is that the flow fields are assumed to be either compressible and gravity-free ($M > 1$, $Fr > 1$) or gravity-dominated and incompressible ($Fr < 1$, $M < 1$). The assumption of incompressible shallow-water flow is good for the Colorado River. However, compressibility and gravity are probably both important for the flow fields of Old Faithful and the Mount St. Helens lateral blast. Using parameters given by *Kieffer* [1981*a*, *b*, 1984*a*], one can demonstrate that in some parts

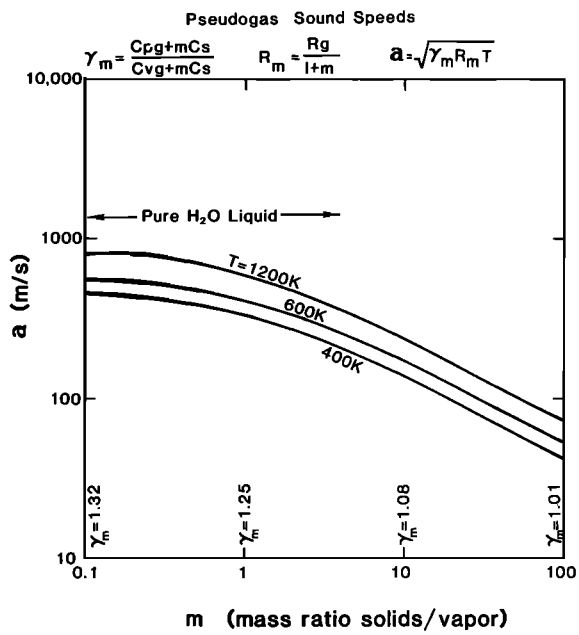

Figure 4. Sound speed a of pseudogas versus mass ratio m of solids to vapor (steam). The pseudogas equations are shown at the top of the graph. The isentropic exponent of the mixture is denoted by γ_m, the heat capacities of the gas phase at constant pressure and volume are denoted by C_{pg} and C_{vg}, and the heat capacity of the solid phase is C_s. The gas constant of the mixture is R_m; the gas constant of the gas is R_g. Curves for three different temperatures spanning the range of geothermal and volcanic interest are shown. The sound speed of pure liquid water is indicated.

of the flow field, $M \sim 1$ and $Fr \sim 1$. In different parts of a flow field, either compressibility or gravity may dominate, and in the discussions that follow the author will point out some limits of the assumptions. The complex problems of flow in which both compressibility and gravity forces are of comparable magnitude and of the magnitude of the second-order effects when one force is dominant are only beginning to be addressed as the capabilities of modern supercomputers are being turned toward the problem.

4. CRYSTAL RAPIDS: SUBCRITICAL AND SUPERCRITICAL FLOW IN AN ERODIBLE CHANNEL

Geologic Setting and the Events of 1983

The Colorado River is the largest of the great rivers in western America. In the 400-km stretch through the Grand Canyon, numerous debris fans have been deposited by flash floods in tributary canyons (Figure 5). Flash floods in the tributaries can carry boulders many meters in diameter into the path of the Colorado River because the gradient of the tributaries is quite steep. When emplaced, the large debris fans temporarily obstruct the path of the river, damming it until the debris deposit is breached and a new channel carved. The major rapids on the Colorado River are located where the river passes through these debris fans.

The channel of the Colorado River resembles a converging-diverging nozzle in the vicinity of these debris fans (note the constriction of the channel in Figure 5). Typically, the channel narrows from a characteristic upstream width of about 100 m to a narrowest point in the "throat" of the rapid, and then diverges back to a downstream width about equal to the upstream width. The ratio of the width of the river at the throat to the width at an average upstream section is herein called the "constriction" of the river or its "shape parameter."

Although the shape parameter is conceptually simple, it is difficult to obtain values that are meaningful for both field and theoretical use because the shape parameter is a function of the discharge rate and because the river channel is complex in three-dimensions. For example, the rise of the river shoreline from the lower (southern) end of the debris fan in Figure 5*a* to the base of the old alluvial terrace (see Figure 5*b* for key) represents a stage change of about 5.5 m and occurs when the discharge increases from about 283 m^3/s (10,000 cfs) to about 2550 m^3/s (90,000 cfs); thus, if the shape parameter were measured at these two extreme discharges, it would have quite different values. The values of constriction shown in Figure 6 were obtained by measuring the width of the surface water in the photograph series of the 1973 U.S. Geological Survey Water Resources Division, one of which is shown in Figure 5*a*. For example, measurements of surface width at Crystal Rapids from Figure 5*a* give a constriction of 0.33,

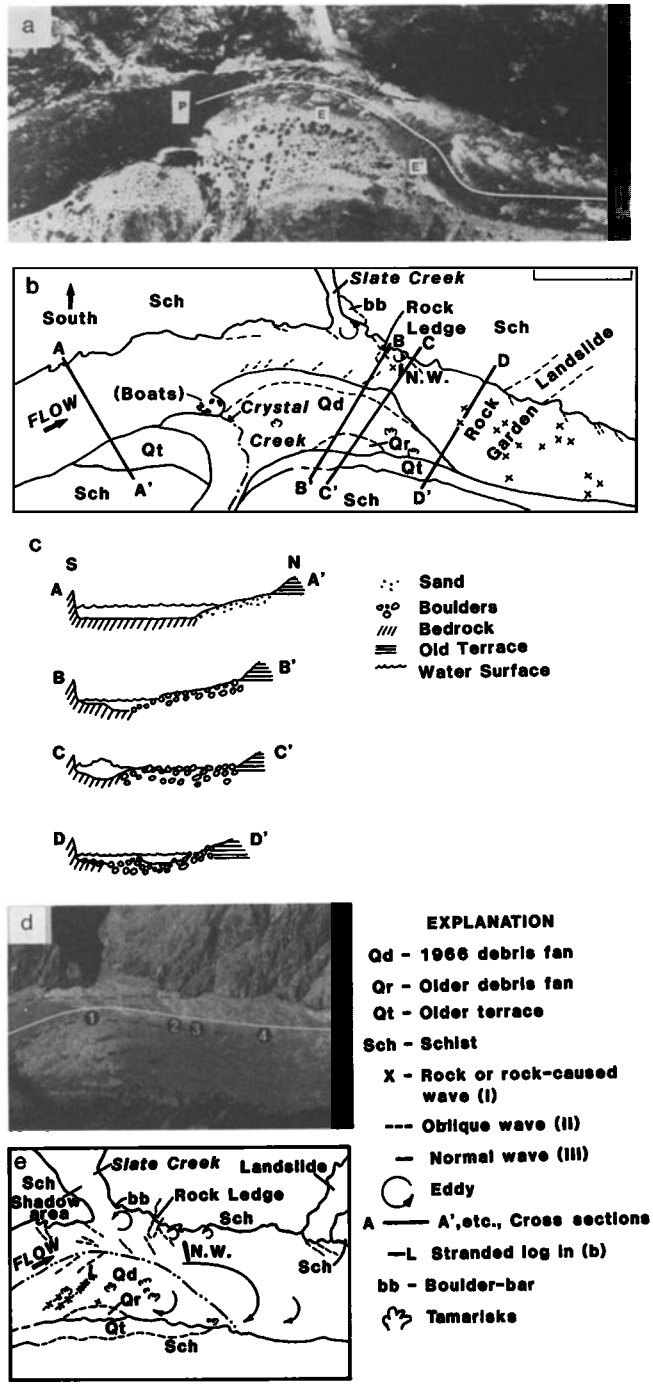

Figure 5. Crystal Rapids at two dramatically different discharges. (*a*) June 16, 1973 (U.S. Geological Survey Water Resources Division air photograph), at a discharge of about 283 m^3/s. (*b*) Keys to features in Figure 5*a*. (*c*) Schematic cross sections, with arbitrary vertical exaggeration. (*d*) June 27, 1983, at a discharge of about 2600 m^3/s. (*e*) Key to features in Figure 5*d*.

which plots as the leftmost block in Figure 6. However, for purposes of hydraulic modeling later in the discussion, it is necessary to assume an idealized cross section for the channel. A rectangular cross section is assumed. In this simplification the "average" constriction used for modeling is generally less than that measured from air photographs,

because the shallow, slow flow across the debris fan, which shows in air photographs of the water surface but accounts for only a small fraction of the total discharge, is ignored. In the case of Crystal Rapids the model value used is 0.25, substantially lower than the 0.33 obtained from surface width measurements.

The debris fans measured to form Figure 6 are generally much older than Glen Canyon Dam, although they are episodically replenished by flash floods from the

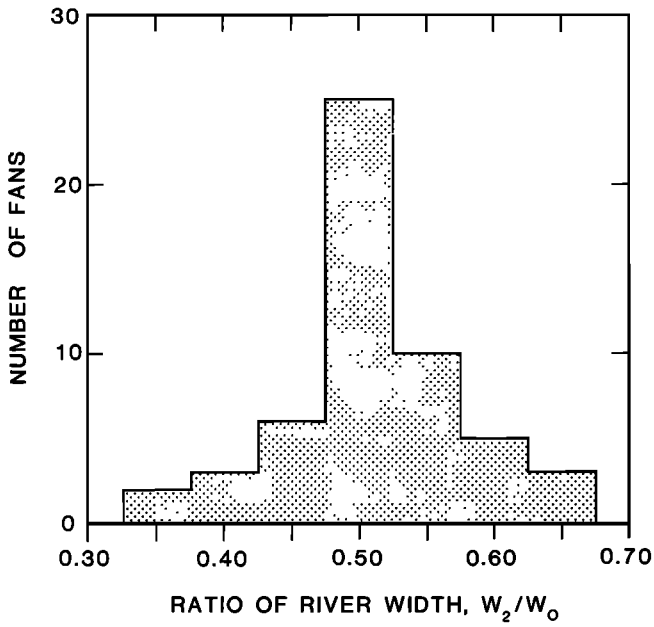

Figure 6. Histogram of constriction values (shape parameter) for the Colorado River as it passes 54 of the largest debris fans in the 400-km stretch below Lees Ferry, Arizona. These values are based on the widths of the surface water in the channel on 1973 air photographs (such as shown in Figure 5*a*).

tributaries. Constrictions at these debris fans are remarkably uniform at a value of about 0.5 (Figure 6), and the tight constriction of Crystal Rapids (at 0.33 in this graph) is almost unique. There is no a priori reason to believe that the debris fans themselves were emplaced in such a way that, by coincidence, half of the main channel was blocked. What, then, is the significance of this characteristic nozzle shape? It must be telling us something about the ability of the Colorado River to erode its own channel, i.e., to contour its own nozzle.

Because the debris fans are generally very old (of the order of 10^3–10^5 years) and because the flash floods that create and renew them are rare, we have little hope of observing the processes that create the balances between tributary floods and main channel erosion. However, a unique series of events spanning the two decades from 1966 to 1986 has given us a glimpse of these processes. In January 1963, Glen Canyon Dam (Figure 7) was closed, and the discharge into the Colorado River through the Grand Canyon became controlled by demands for electrical power and water storage at the dam, rather than by natural flooding. About 4 years after the dam was closed, a flash flood down Crystal Creek emplaced a large debris fan across the river (Figure 5) about 175 km below the dam. There were no witnesses to this event; by the time observations were made, the Colorado River had carved a channel through the distal (south) end of the debris fan. When first measured (on the 1973 air photograph shown in Figure 5*a*), the constriction of the river channel through the fan was roughly 0.33, substantially more severe than the constrictions of the more mature fans along the Colorado River. From 1966 to 1983 the constriction remained at about 0.33. During this time, discharges through the dam were held below 850 m^3/s.

The water surface of the Colorado River became very rough and turbulent as it passed through the Crystal debris fan; this stretch of water, nearly 1 km long, is known as Crystal Rapids. The boulders, waves, and eddies in Crystal Rapids made it one of the two most difficult stretches of the river for raft navigation, even at the normal levels of controlled discharges between 1966 and 1983 (140–850 m^3/s). The rapid is a major hazard for recreational rafting, an activity in the Grand Canyon involving about 10,000 people each year.

The schematic cross sections in Figure 5*c* show the cause of the navigational difficulties from another perspective. In the backwater and convergent reach (cross

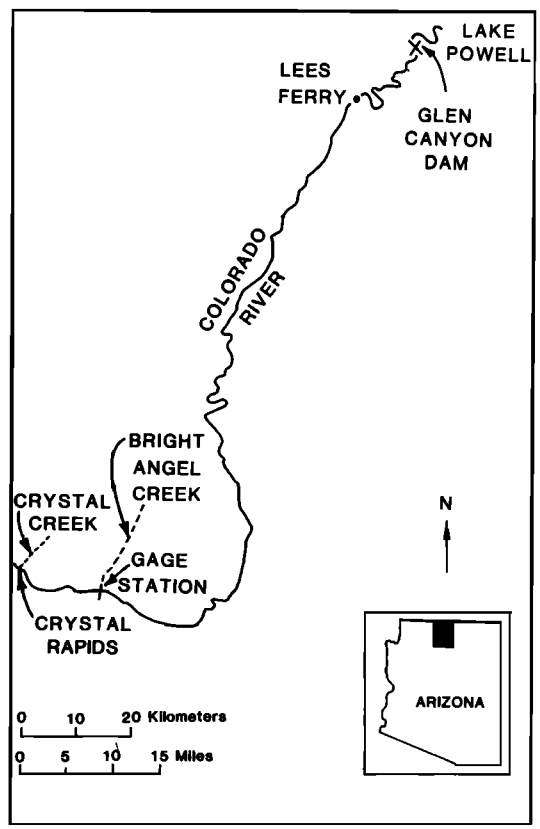

Figure 7. Index map for locations near Crystal Rapids.

section A-A′) the water is relatively deep and slow. In the constricted sections (cross sections B-B′ and C-C′) the flow is shallow and fast, thus exposing many rocks (in cross section C-C′ the wave discussed below is shown much exaggerated vertically). Even in the divergent reach (cross section D-D′) where the river is somewhat wider and the gradient is less steep, the water still flows fast. Because the channel bottom is rocky at the downstream end of many rapids (see discussion below), this section of the river channel is also difficult for raft navigation, and many a river runner can tell tales of spending hours, or even an unpleasant night, stranded on the rocks near D-D′.

Between 1966 and 1983 the major navigational obstacle occured where water poured over a large rock into a deep hole and emerged through a sharp-crested wave in the narrowest part of the rapid. (The preferred navigation route during this time is shown by the line P-P′ in Figure 5*a*.) This feature was known as the "Crystal Hole" (the location of the Crystal Hole is shown in Figures 5*b* and 5*e* by the notation N.W., which stands for "normal wave," but the feature itself is too small and too blurred by turbulence to show at the scale of the photographs in Figures 5*a* and 5*d*).

At low discharges, a rock about 2 m high was seen at the Crystal Hole, and most observers believed that the rock was the sole cause of the wave. The relative importance of the rock to the hydraulic effect of the severe constriction was, in hindsight, overestimated. Many waves in the rapids of the Colorado River are indeed caused solely by large rocks. It is well known from river guides who ran the river before Glen Canyon Dam was closed that when large natural floods reached 2300–3600 m^3/s annually, the waves in most rapids became very weak or even disappeared ("washed out"). The wash-out occurred at high discharges because the obstacles causing them become submerged ("drowned"). There was, however, no record of the behavior of waves in Crystal Rapids at discharges exceeding 850 m^3/s, because the rapid, in its modern servere form, did not exist before construction of Glen Canyon Dam.

In 1983, rapid snowmelt in the headwaters of the Colorado River forced the Bureau of Reclamation to increase discharges through Glen Canyon Dam to 2600 m^3/s to prevent Lake Powell from flowing over the dam. As discharges increased above 850 m^3/s (a level that had not been exceeded for two decades) the waves in most rapids disappeared, as expected. The rapids "drowned out" and the river ran smooth and fast through most of the Grand Canyon.

This was not the case at Crystal Rapids: as the discharge reached 1700–2000 m^3/s, a wave reported by experienced river guides to have been as high as 9 m, and photographically documented to have exceeded 5 m, stood across much of the river channel (Figure 8). At greater discharges the height diminished: at 2600 m^3/s the wave surged only between 3 and 5 m. Because typical river rafts are 5–11 m in length and 2–4 m in width, the wave was a severe obstacle to boating. One rafter was drowned, and dozens of others were seriously injured. The National Park Service closed the rapid to commercial boating until the discharges were decreased. The existence of this large wave at high discharges, and its evolution with changing discharge, provided clues about the relation between the Colorado River and its debris fans.

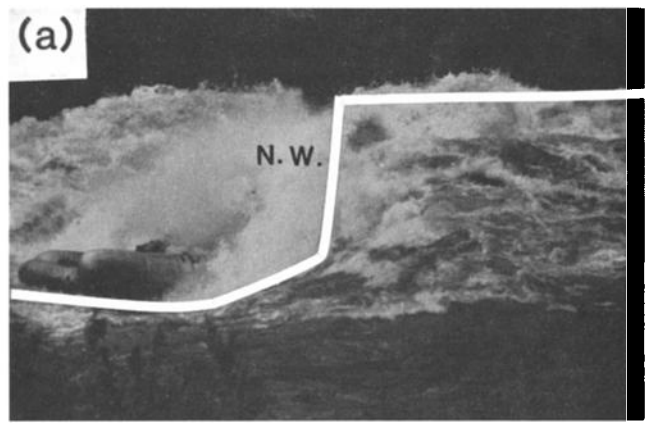

Figure 8. River raft (*a*) entering and (*b*) trapped in the large wave at Crystal Rapids on June 25, 1983, when the discharge was approximately 1700 m^3/s. Pontoons on the raft are each 1 m in diameter; the midsection is about 3 m in diameter. More than 30 passengers are on board (one head is visible on the lower left side of the raft in Figure 8*b*). To aid the reader in distinguishing between the water surface near the boat and in the foreground from the turbulent water in the background, a white line has been drawn along the approximate surface of the water upstream from and through the hydraulic jump in Figure 8*a*. For explanation of N.W., see Figure 5. From the scale of the raft, the trough-to-crest height of the wave can be estimated to exceed 5–6 m. (Photographs copyrighted by Richard Kocim; reprinted with permission.)

Results of Analysis of Shallow Water Flow

Certain aspects of the flow in the rapids of the Colorado River can be analyzed in terms of conservation of mass and momentum for flow in a converging-diverging

channel [*Kieffer*, 1985]. As discussed in the context of Figure 2, the shape of the channel, and the upstream and downstream reservoir heads, must be specified, and the properties of the flow field in different parts of the channel can then be calculated. Six different flow zones can be identified, as shown in Figure 9*a*: (0) an upstream state of unconstricted, uniform flow, (1) the convergent section of the channel upstream from the constriction, (2) the constriction, (3) the beginning of the divergence, (4) the end of the divergence, and (5) a downstream state of uniform flow not influenced by the constriction. Regions (3) and (4) may be separated by a hydraulic jump.

Water flows through the rapid because the upstream reservoir is higher than the downstream reservoir.

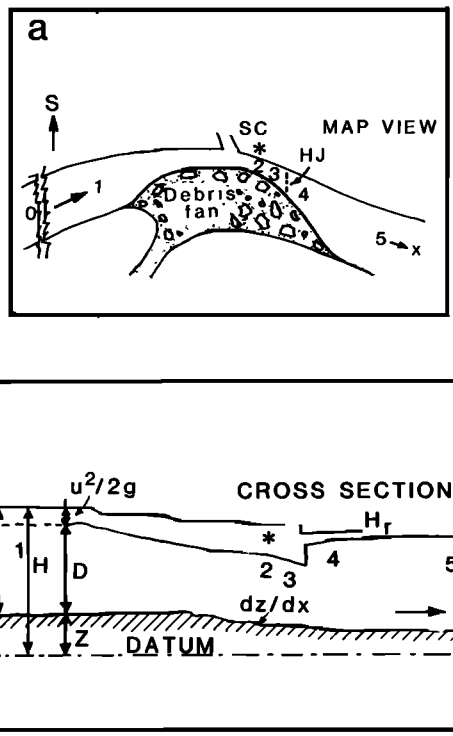

Figure 9. (*a*) Schematic map view of the river and the debris fan configuration at Crystal Rapids. HJ indicates a possible hydraulic jump. (*b*) Schematic longitudinal profile, showing notation used in the energy relation given in the text and in Figure 10. WS indicates water surface.

Application of the Bernoulli equation to any two cross sections 1 and 2 gives the total energy balance as

$$z_1 + D_1 + \frac{u_1^2}{2g} = z_2 + D_2 + \frac{u_2^2}{2g} + E \qquad (16)$$

where E is the energy dissipated between sections 1 and 2. The notation here has been slightly changed from that used in the general equations of section 2 to be consistent with Figure 9; the change in convention from the variable h used in section 2 for water depth to the variable D is required to account for a sloping channel bottom by referencing both the channel bottom and the water surface to a datum plane as in Figure 9*b*. For simplicity, and because of a paucity of data, the energy change due to the change in bed elevation ($z_1 - z_2$) is assumed to be compensated by energy dissipation in the flow, E. This assumption allows the flow to be considered at constant specific energy ($D + u^2/2g$), except across hydraulic jumps. For the analysis the discharge variation of the specific energy of the unconstricted flow upstream of Crystal Rapids was estimated from measurements at the U.S. Geological Survey gage station 16 km upstream at Bright Angel Creek (Figure 10*a*, heavy line, H_r). The flow below Crystal Rapids was assumed to return to this same specific head.

The flow entering the rapid can have the ambient specific head H_r if, and only if, all of the discharge can be accommodated through the constriction. If the constriction is too severe, the ambient head of the flow, H_r, may not be sufficient to allow the discharge to be accommodated through the constriction. In such cases, critical conditions occur in the constriction, and a backwater is required upstream. The deepening of the backwater increases the specific head of the flow over that in the unconstricted part of the channel and permits a greater discharge per unit area through the constriction. The calculated backwater head H_b compared to the ambient river head H_r is shown as a function of discharge Q and constriction value in Figure 10*a*. Note from this figure that for a constriction of 0.25 a backwater head is required for all discharges over about 300 m^3/s; the backwater above Crystal Rapids is so big that it has been affectionately dubbed "Lake Crystal" by river runners. This calculation means that supercritical flow will occur in the rapid at discharges above a value of approximately 300 m^3/s.

Solutions of the shallow-water flow equations are shown in Figures 10 and 11. In each part of Figure 10 a calculated or measured parameter is shown as a function of discharge on the abscissa and the shape parameter (labeled on each curve separately). In Figure 10*a* the specific head of the unconstricted river (H_r) and the backwater head (H_b) that develop upstream of Crystal Rapids for conditions of critical (choked) flow are shown. In Figure 10*b* the calculated and observed heights of the hydraulic jump (normal wave, N.W., in Figures 5 and 8) are shown. Figure 10*c* shows three important variables: (1) the flow velocity in region 3 just upstream from the hydraulic jump (upper, solid curves), (2) the flow velocity in region 4 just downstream from the hydraulic jump (lower, dashed curves), and (3) a heavy straight line at 9 m/s that indicates the velocity chosen as a threshold velocity at which the large boulders of the Crystal debris fan would be moved (see *Kieffer* [1985] for a discussion of this and more details on this figure). Figure 10*d* shows the velocity in region 2,

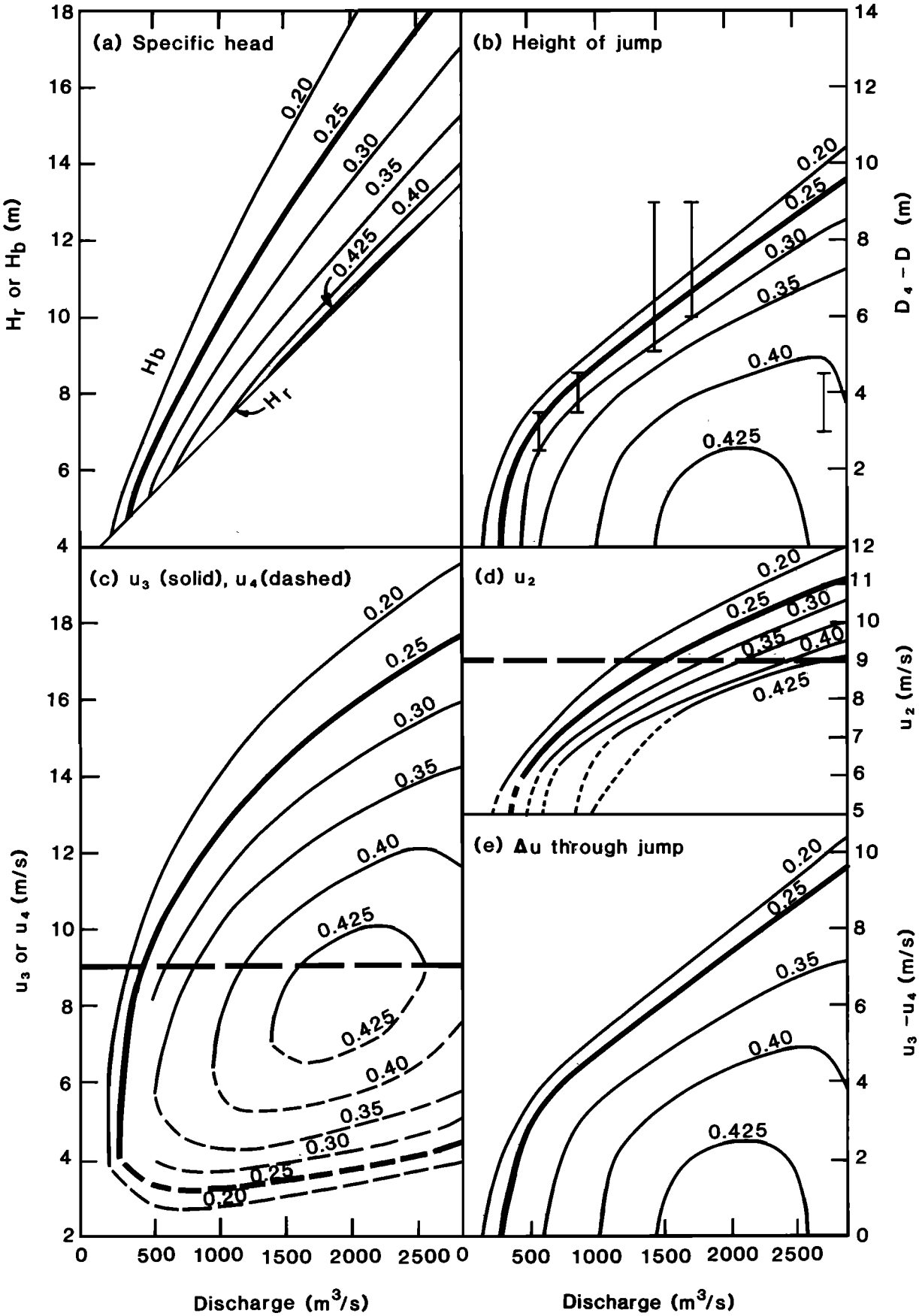

Figure 10. Summary of the shallow-water flow calculations for Crystal Rapids given by *Kieffer* [1985].

the constriction, and the reference line at the threshold velocity of 9 m/s. Figure 10*e* shows the change in velocity ($u_3 - u_4$) through the hydraulic jump. In all parts of Figure 10 the curve appropriate to the geometry of the rapid prior to 1983 (shape parameter, 0.25) is shown as a heavy line.

Careful inspection of the different parameters in the parts of Figure 10 shows that Crystal Rapids went through the entire spectrum of nozzle behavior shown in the sketches of Figure 2 as discharges increased during the 1983 flood. For example, at low discharges and small shape factors (tight constrictions) the flow was essentially subcritical; this can be seen in Figure 10*a* by the fact that there is no backwater head at low values of discharge, and in the other figures by the absence of hydraulic jumps and their associated velocity changes at low discharges. These ideas are summarized more graphically in Figure 11, which shows schematic longitudinal water surface profiles and channel bottom configurations. The bottom level of the channel changed with discharge in 1983 because of erosion; the decreases shown are those measured 16 km upstream at the Grand Canyon gage station. In this figure the five curves and bed elevations represent the following conditions: **A**, 283 m^3/s and moveable bed **A**; **B**, 850 m^3/s and same bed level as **A**; **C**, 1400 m^3/s with bed lowered by 1 m relative to the bed of **A** and **B**; **D**, 1700 m^3/s with same bed as **C**; and **E**, 2550 m^3/s with the bed lowered 1 m relative to the bed of **C** and **D**, possibly to a fixed (bedrock?) position. Curve **A** shows subcritical flow conditions. Curves **B**–**E** all show supercritical flow conditions. For these conditions, the height of the hydraulic jump and the velocity change across it are given beside the vertical line representing the jump.

At discharges below about 300 m^3/s the flow was essentially subcritical (curve **A** in Figure 11). At higher discharges the flow became critical and then highly supercritical (curves **B**–**E** in Figure 11). The reader should note the specific use of the past tense in the last two sentences, because the events of 1983 modified Crystal Rapids, and these calculations are not appropriate to its current configuration.

A hydraulic jump is required in the diverging section of the rapid to decelerate the supercritical flow and to drop its energy from the backwater head H_b back to the ambient downstream head H_r. Thus the model suggests that the large wave that stood in the diverging section of Crystal Rapids at high discharges can be interpreted as a normal hydraulic jump arising from the severe constriction of the channel (Figure 2). In hindsight, this wave can be recognized as having been present all through the 1966–1983 phase of Crystal Rapids. However, because the large rock in this vicinity acted as a small-scale natural weir, the energy change of the flow around the rock

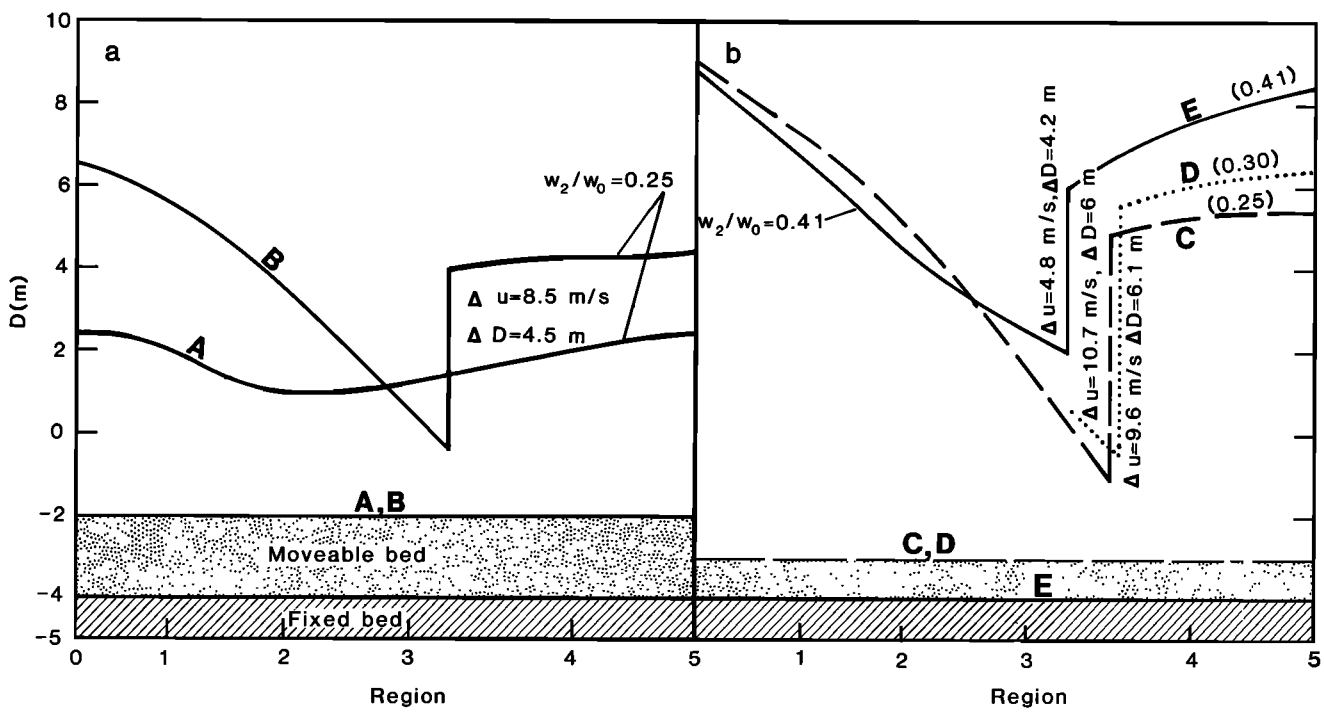

Figure 11. Schematic longitudinal water profiles at Crystal Rapids for the 1983 discharges up to 2550 m^3/s, showing the effect of channel widening and bed erosion on the height of the hydraulic jump. The parts of the rapid (regions 0–5) defined in the text and in Figure 9 are shown schematically by the labels below the graph. Discharge conditions for curves A–E are discussed in text.

contributed substantially to the energy of the wave at low discharges, so that the role of the constriction was not recognized. Only when the wave strengthened with increasing discharge, rather than washing out, was the role of the constriction recognized.

As the discharge through Glen Canyon Dam rose from 850 m^3/s to about 1700 m^3/s in June 1983, the height of the wave increased, as would be expected for a hydraulic jump in a channel of fixed geometry (in Figure 10*b*, compare the left four data bars with the heavy curve). At higher discharges, however, the height of the wave decreased, rather than increasing as predicted by the calculations (in Figure 10*b*, compare the right data bar with the heavy line).

This puzzling observation can be explained if the magnitudes of the flow velocities in the constriction and upstream of the hydraulic jump are examined (Figures 10*c* and 10*d*; see also the profiles in Figure 11). In supercritical flow, water accelerates in the converging section of the nozzle, reaching critical velocity u_2 in the throat. The water continues to accelerate out the diverging side of the constriction, reaching a maximum velocity u_3 immediately upstream of the hydraulic jump. A sudden deceleration to velocity u_4 occurs across the hydraulic jump as the flow deepens. For example, at a discharge of 1400 m^3/s with a constriction of 0.25, the calculated velocity in the constriction, u_2, is 9 m/s and the velocity increases to $u_3 = 14$ m/s just upstream from the hydraulic jump (Figures 10*c* and 10*d*). The velocity decreases to $u_4 \sim 3$ m/s just downstream from the jump.

Consideration of the Hjülstrom criterion for particle movement [*Hjülstrom*, 1935] and of unit stream power shows that water moving at 9 m/s can move boulders that are 1–2 m in diameter, the characteristic size of the large boulders of the Crystal debris fan. Therefore when velocities reached this magnitude (at discharges in the range of 1400–2000 m^3/s as shown in Figure 10), large-scale erosion began; that is, the river was able to begin contouring its own nozzle. Material was eroded from the sides of the channel and from the river bottom. Vertical erosion scoured the channel in an upstream direction (headward erosion); lateral erosion increased the width of the throat. An observer standing on the shore could not see this erosion taking place but could hear loud, bass booms as boulders moved in the current.

Channel widening at the throat can account for the observed decrease in height of the hydraulic jump. Comparison of the observed wave height with that predicted for a normal hydraulic jump as the discharge changed from 1700 to 2600 m^3/s suggests that the channel widened from a shape parameter of 0.25 to about 0.40–0.42, a widening of 12–13 m (Figure 10*b*). The proposed erosion was difficult to document because discharges were kept relatively high (of the order of 1400 m^3/s) for nearly a year after the peak discharges in the summer of 1983. Nevertheless, photographic evidence (Figure 12) suggests that this erosion did occur and that it, in fact, occurred in and downstream of the constriction, just where this model suggests velocities should have been the highest. In Figure 12, note a large rock, indicated by an arrow in both photographs, and the widening of the channel immediately downstream (right) of the rock in Figure 12*b*, taken after recession of the high water.

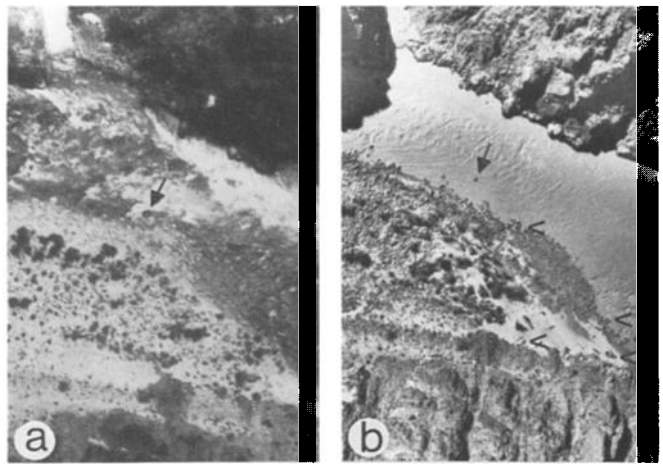

Figure 12. Comparison of the shoreline at Crystal Rapids (*a*) before and (*b*) after the 1983 high discharges. The text discusses erosion along the shoreline between the rock indicated by the arrow and the boats indicated by V's in Figure 12*b*.

(Comparison of these photographs is a bit difficult because the discharge in Figure 12*a* is about 283 m^3/s and in Figure 12*b* is about 170 m^3/s. Even though the discharge is lower in Figure 12*b* than in Figure 12*a*, boats (indicated by V's) can be seen in an "alcove" in Figure 12*b*, a position they could not have obtained at the discharge shown in Figure 12*a*, even though there is a higher stage in Figure 12*a* that should have submerged the rocks in this vicinity. This suggests that rocks were indeed removed from this vicinity.) Additionally, in the field it can be observed that there is a fresh cut bank nearly 2 m in height along the area that is indicated schematically as regions 2 and 3 in Figure 9; this cut bank is visible as a faint line to the left side of the boats in Figure 12*b*. Similar cut banks are now being recognized as signs of river channel erosion at a number of rapids where there have been fresh debris flows (Granite Rapids, Elves Chasm) and indicate the powerful ability of the river to cut its own channel.

In a channel with a nonerodible bed the flow velocity would be expected to increase with discharge, but in this situation where the river channel was erodible, the flow

velocity becomes fixed at the threshold for erosion. This number was chosen somewhat arbitrarily on the basis of the Hjülstrom criterion as discussed above, but it is consistent with the only available measured velocities. Three kayaks were filmed going through the rapid on June 27, 1983, when the flow was 2600 m^3/s. The trajectory for the one kayak for which the best data were obtained is shown in Figure 5*d*. Measured velocities were as follows: immediately upstream of point 1, 8.5 m/s; point 1 to point 2, 9.8 m/s; point 3 to point 4, 8.7 m/s. The kayak stalled to an average velocity of 3.3 m/s between the trough and crest of the hydraulic jump in this region before accelerating down the backside of the wave to a velocity of about 8.5 m/s.

In summary, a fascinating, and often tense, feedback process involving meteorology, river hydraulics, and engineers began in June 1983 and continued into early July as the discharge increased; this process can be followed on the curves of Figure 10. As snow melted in the Rocky Mountains, engineers raised the discharge through the dam higher than the 850 m^3/s released during the previous two decades. At the tightly constricted spot in Crystal Rapids, a large hydraulic jump formed because the flow became highly supercritical. As the discharges approached 1700 m^3/s, the river began eroding its channel through the Crystal Creek debris fan. In response to the widening, the flow velocities decreased. If the discharge had been held constant, the channel and hydraulic features of the flow would have stabilized when the channel became wide enough to reduce flow velocities in all sections below about 9 m/s. However, more snow melted in the headwaters of the Colorado River, and engineers were forced to increase discharges through the dam toward 2600 m^3/s. In response to the increased discharge, flow velocities again increased, and erosion of the channel continued; by the time of peak discharge, enough lateral erosion of the channel had occurred that the height of the hydraulic jump had decreased. It is not clear at this time whether the high flows were sustained long enough for the channel to take on a shape in equilibrium with the high discharge.

Implications for Geomorphic Evolution in the Grand Canyon

Even after the channel was widened by the high discharges of 1983, the constriction of 0.40–0.42 at Crystal Rapids is still significantly below the value of 0.5 characteristic of the mature debris fans along the Colorado River (Figure 6), and the rapid is significantly different in hydraulic character from rapids at locales where the constriction is 0.5. This observation suggests that most debris fans in the Grand Canyon have been subjected to floods larger than the 1983 flood. With proper recognition of the simplicity of the model and the paucity of data, extrapolation of calculations at Crystal Rapids can be used to estimate that a flood of 11,000 m^3/s might have been required to enlarge the constrictions to the value of 0.5 observed for most debris fans [*Kieffer*, 1985]. This is not an unreasonable value, because it is known that a flood of 8500 m^3/s occurred in 1884.

The calculations described here attribute all changes in flow regime to lateral constriction, because of the assumption of constant specific energy. In all rapids there are changes in bed elevation that affect the total and specific energy of the flow and, therefore, affect the transitions from subcritical to supercritical conditions. The words "subcritical" and "supercritical" as used in this section, and in the following summary, therefore apply to a large-scale description of the rapid, not to local details, because these additional effects are not accounted for. Most rapids are weakly supercritical because of changes in bed elevation, even in the regime called "subcritical" in this paper. There are also substantial small-scale irregularities in bed topography, such as ledges and rocks, that cause local supercritical flow. The behavior of the river around such obstacles is not included in this generalized discussion.

The calculations indicate that when constrictions of the Grand Canyon debris fans reach the value of ~0.45, the flow will be essentially subcritical at all discharges. Although some standing waves and local regions of supercritical flow exist in most of the rapids of the Grand Canyon, the wave at Crystal Rapids was unique: other rapids that are less tightly constricted do not have strong normal waves (river rafters might disagree, because many of the existing waves are strong enough to flip rafts, but—at the scale of convergent-divergent constrictions considered here—these are local features).

Over geologic time, the flow in Crystal Rapids can change from subcritical to supercritical (or vice versa) in two ways: (1) as discharge changes from season to season in a channel of fixed constriction, or (2) as channel constriction changes with time because of erosion during large floods or because of tributary debris flows. This evolution is summarized in Figure 13, a version of Figure 2 that shows explicitly the response of channel shape and flow structures to changes in discharge. The sequence shown represents but one cycle in recurring episodes in which debris fans are enlarged by floods in the tributaries and then modified by floods in the main channel.

The beginning of the sequence is arbitrarily chosen as a time when the main channel is relatively unconstricted (Figure 13*a*). The river is suddenly disrupted and ponded by catastrophic debris fan emplacement (Figure 13*b*), forming a "lake" behind the debris dam. The surface over which water pours across the freshly emplaced debris fan is called a "waterfall" in this model. As the ponded water overtops the debris dam, it erodes a channel, generally in the distal end of the debris fan (Figure 13*c*). This is the

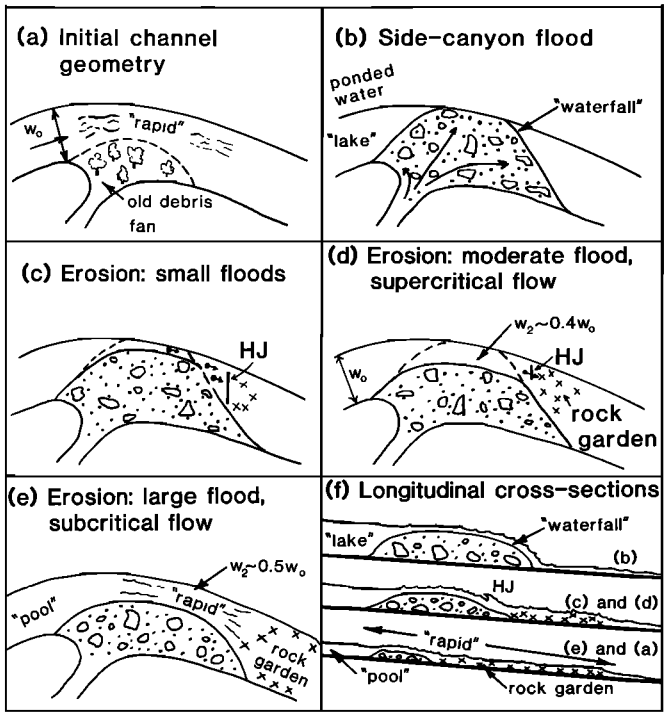

Figure 13. Schematic illustration of emplacement and modification of debris fans in the Grand Canyon, modeled after the processes observed at Crystal Rapids during 1966–1983. HJ indicates a hydraulic jump; w indicates river width, with the subscripts 0 and 2 standing for regions 0 and 2 as defined in Figure 9*a*.

beginning of evolution of a "rapid" from a "waterfall." Observations of naturally emplaced earth dams suggest that the breaching of the Crystal debris dam probably happened within hours or days of its emplacement.

Unless the debris dam is massively breached by the first breakthrough of ponded water (that is, unless enough material is removed that the shape parameter is initially greater than 0.5), the constriction of the river is initially severe. Floods of differing size and frequency erode the channel to progressively greater widths (Figures 13*c*, 13*d*, and 13*e*). Small floods enlarge the channel slightly, but constricted, supercritical flow is still present (for example, as in Crystal Rapids from 1966 to 1983). Moderate floods enlarge the channel further (perhaps to a constriction $w_2/w_0 \sim 0.4$). The geometry observed at any instant reflects the largest flood in the history of the fan (for example, floods of 11,000 m^3/s appear to enlarge the constrictions along the Colorado River in the Grand Canyon to a shape parameter of about 0.5). At any time, depositional events in the main channel or the tributaries may complicate this simple description of the erosional history.

Rocks from the debris fan are transported as far as 1 km downstream by the high-velocity water in the convergent, constricted, and divergent regions. Notice, in Figure 5*a* (and in its explanation, Figure 5*b*) that there is a deposit of rocks, labeled "rock garden," below the divergent stretch of the rapid. Rocks in the rock garden in Crystal Rapids are visible at 285 m^3/s, cause substantial waves at 850 m^3/s, and are submerged at 2600 m^3/s (as shown in Figure 5*d* and its index Figure 5*e*). Rock gardens like this can be found below a number of major rapids in the Grand Canyon (for example, below Granite Rapids and Bright Angel Rapids). This theory suggests that the rocks that form the rock gardens have been transported there from the original debris fan deposits under a range of different fluid flow conditions as the Colorado River has progressively enlarged its channel during big floods (Figures 13*c*–13*f*).

Mature debris fans that once blocked the Colorado River and now have channels cut through them have progressed with time from the bottom to the top of Figure 2 (or, cyclically, from Figure 13*a* to 13*e*), because natural floods have been large enough to create subcritical channels from the initially supercritical constrictions. Controlled discharges through Glen Canyon Dam will not permit Crystal Rapids to evolve to the configuration of the older debris fans. However, the controlled releases from the dam (1415 m^3/s when only the generators and bypass tubes are used, greater values if the spillways are used) are sufficient to significantly alter the channel of the river should it become blocked or tightly constricted by tributary floods in the future.

What perspective does this interpretation of the history of the hydraulics and geomorphology of the Colorado River give us? First, the interpretation of a major wave as a hydraulic jump arising not from a rock but from large-scale channel geometry provides a different perspective for monitoring and predicting events at newly formed rapids, a perspective valuable for National Park Service officials concerned with navigational safety. Any rapid newly formed by a debris flow may exhibit hydraulic features different from those seen in channels through older debris fans because of the severe constriction that can be present. Such rapids should be monitored closely if unusually high discharges are put through Glen Canyon Dam.

Second, the interpretation of critical flow in the constriction and supercritical flow downstream from the constriction predicts erosion in quite different places than would be found in a subcritical nozzle, and the interpretation of the shape of the river channel allows modeling of sizes of ancient floods. Interpretation of the flow in this way also allows a mechanism for transporting large boulders a significant distance downstream from the original debris deposit into rock gardens because of the high velocities that can occur downstream of the constriction in supercritical flow. Without such a mechanism, geologists are faced with the dilemma that tributary debris flows from side canyons are building weirs across the canyon, and downcutting through these weirs is difficult because only local abrasion or chemical solution can be

invoked to get rid of the rocks. The relative roles of local abrasion, solution, and downstream transport of large particles must be understood before quantitative models of infilling versus downcutting of the Grand Canyon can be formulated.

Finally, the framework of supercritical to subcritical evolution of the rapids with time and through flood events of different sizes suggests new directions for geologic and hydraulic observations at the rapids: searches for geologic evidence of the estimated 11,000 m^3/s prehistoric flood (even traces of the historic 8500 m^3/s flood are difficult to find); evaluation of the relative roles of lateral constriction versus vertical topography on the channel bottom; documentation of wave behavior as discharge changes; laboratory experiments on the three-dimensional shapes of hydraulic jumps in flumes of converging-diverging geometry; development of criteria for transport of large boulders (>1 m diameter) by fluids (a research topic that will be discussed again in the concluding section of this paper on the Mount St. Helens lateral blast); and evaluation of the relative frequencies of tributary versus main stem floods in determining the rate of downcutting by the Colorado River within the Grand Canyon. A new data base for these studies is available in the form of detailed maps of the topographic and hydraulic features of the Colorado River channel in 10 important locations: at House Rock, 24.5-mile, Hance, Cremation-Bright Angel, Horn Creek, Granite, Hermit, Crystal, Deubendorff, and Lava Falls Rapids [*Kieffer*, 1988].

5. OLD FAITHFUL GEYSER: A TWO-PHASE NOZZLE

Geologic Setting

Reports of geysers and hot springs in the land that is Yellowstone National Park began in the early part of the nineteenth century. Old Faithful Geyser has since become a familiar symbol of the western lands of the United States and their national parks (Figure 14). More recently, Old Faithful became an important focus of scientific studies when striking resemblances between a peculiar type of volcanic seismicity known as "harmonic tremor" (Figure 15*a*) and the seismicity of the geyser were noted and explained (Figure 15*b*) [*Kieffer*, 1984*a*]. Figure 15*b* shows a seismic record of about 1 day of eruptions at Old Faithful, showing 11 complete eruption cycles (a higher-resolution record of one complete eruption cycle is shown in Figure 20 and is discussed in detail later in this section). Each active period of seismicity of Old Faithful ends with an eruption and a characteristic eruption coda (a good example of an eruption coda is on line 11, beginning between the first and second time marks and extending to the fourth). The similarity of the record from Karkar Volcano (Figure 15*a*) to geyser records such as that of Old Faithful led *McKee et al.* [1981] to suggest that underground geyser eruptions were occurring at Karkar.

Figure 14. Old Faithful geyser, Yellowstone National Park, in eruption. The column is about 30 m high. Note the discrete elements of fluid in the eruption column. These are the "surges" referred to in the text. Photograph by G. Mendoza.

Harmonic tremor is a relatively monochromatic seismic motion that often precedes or follows volcanic eruptions; as a precursor it has been invaluable in forecasting eruptions, even though no theory has adequately explained its origin. Harmonic tremor is also an important component of the seismic noise characteristic of geothermal fields, and it is thus potentially an important prospecting tool for geothermal energy sources, sources that may provide only a few percent of the total energy requirement of the United States but that could provide a substantial and critical portion of the energy requirements of many countries surrounding the Pacific basin. In this section I summarize my observations and theory for the origin of harmonic tremor at Old Faithful, the importance of fluid properties in interpretation of the data, and my ideas about the complex process that occurs when the geyser erupts.

For perspective, a fluid dynamicist might imagine Old Faithful as a vertical, open-ended, two-phase shock tube with variable cross section. In addition to the compressibility effects that normally dominate shock tube dynamics, gravitational (hydrostatic) effects strongly influence the fluid properties in the geyser, because each meter of liquid water (providing approximately 0.1 bar

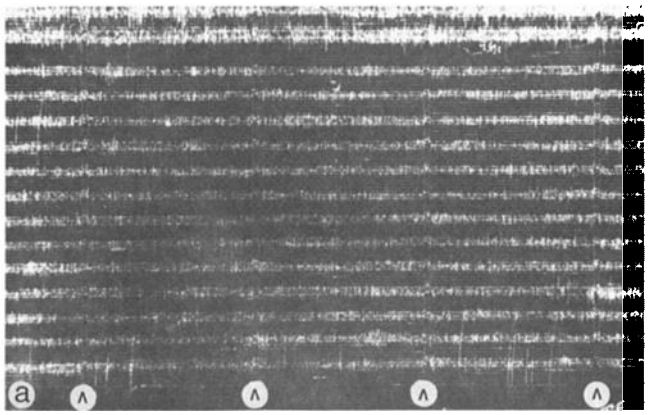

Figure 15. (*a*) A seismic record from Karkar volcano, Papua New Guinea. The white bands are strong seismic activity at a frequency of 2–4 Hz. The pattern recurs at intervals of about 70 min. (*b*) A seismic record of about 1 day of eruptions at Old Faithful. Time marks in both records indicate 1-min intervals; inverted V's in Figure 15*a* emphasize faint time marks. (Figures courtesy of C. McKee and R. W. Johnson [see *McKee et al.*, 1981].)

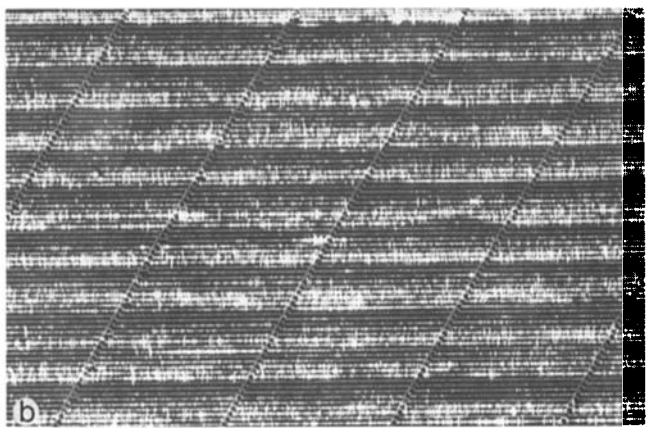

pressure) changes the boiling temperature of the fluid by about 2°C. Thus, in contrast to a shock tube in which initial conditions are usually isothermal and isobaric, the initial pressure and temperature conditions in Old Faithful are not uniform. The recharge cycle of the geyser is analogous to the process of filling a shock tube driver section with a volatile liquid, such as liquid Freon, that can boil upon decompression. At Old Faithful, however, there is no physical diaphragm to contain the fluid as there is in a laboratory shock tube. The natural diaphragm is the highest water in the conduit that maintains a temperature of 93°C (the boiling temperature at the 2200-m elevation of Old Faithful) and sufficient pressure to keep deeper water from massive boiling and eruption. Finally, whereas in the laboratory an experimenter would worry about the "cleanliness" of eruption initiation over time scales of microseconds to milliseconds, at an eruption of Old Faithful we may be lucky to forecast the initiation time of an eruption to within 10 min!

Study of this complex shock tube must be done under very restricted conditions. Whereas a major problem in the study of the Colorado River discussed in the preceding section is inaccessibility, an equally major problem in studying Old Faithful geyser is its accessibility and public visibility. Observations close to the vent must be made on the few days of the year when work will not detract from tourists' enjoyment of the geyser (namely, when Yellowstone Park is closed for snowplowing of the roads in late winter), and experiments or observations must be designed to avoid even the slightest damage to the geyser (for example, no hole can be dug to allow positioning and anchoring of a seismometer). Thus the challenge in studying Old Faithful is to learn as much as possible about the inner workings of a complex nozzle from very limited observations. The basic data set consists of float and thermocouple measurements made in 1949 [*Birch and Kennedy*, 1972], seismic and movie data taken from 1976 to 1984 [*Kieffer*, 1984*a*], and unpublished pressure and temperature data that J. Westphal and I obtained in 1983 and 1984 (summarized by *Kieffer and Westphal* [1985]).

The Recharge and Eruption Cycle

Old Faithful erupts into a tall, continuous vertical jet of water and steam (Figure 14). The maximum height of the geyser ranges between 30 and 50 m, depending mostly on wind velocity and, to a certain extent, humidity (which affects the visibility of vapor in the eruption). Eruptions last for ~1.5–5.5 min and occur every 40–100 min (Figure 16). Measurements of total discharge suggest that about 0.114 m^3/s (114 kg/s; 1800 gal/min) is erupted during the initial and steady-flow stages of the eruption (E. Robertson, U.S. Geological Survey, private communication, 1977).

The conduit of the geyser, or the nozzle, is a fissure that is flared at the surface, narrows to a constriction at about 3–5 m depth, and probably diverges into one or more caverns below this depth. (Figure 17 shows a possible configuration based on calculations described by *Kieffer* [1984*a*]; available data permit many other configurations, so the shape shown in this figure should be considered highly schematic.) About 0.5 m below the rim of the geyser the fissure is 1.52 × 0.58 m, and I will take these as the dimensions of the exit plane of the fluid because the actual geyserite surface is very irregular (including a petrified tree stump visible as the knob on the left side of the cone in Figure 14). Probe work by J. Westphal, R. Hutchinson, and S. Kieffer (unpublished data, 1983, 1984) suggests that the constriction dimensions are approximately 0.1 × 1.5 m. The depth of the conduit that can be reached by a probe is 22 m (this region is called the "immediate reservoir"); it is plausible that water from greater depths is ejected during a long eruption. Water fills the conduit only to within 6 m of the surface (Figure 17).

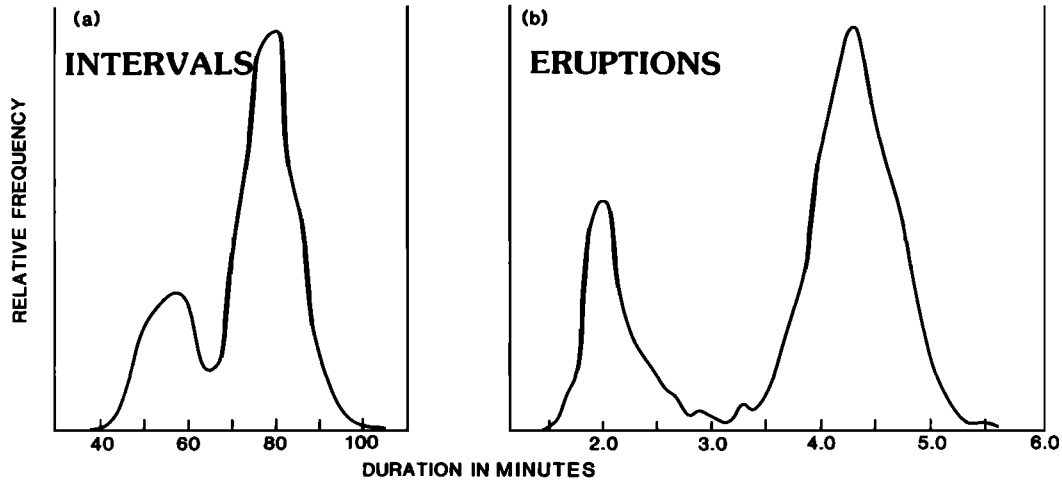

Figure 16. (*a*) The relative frequency of intervals between eruptions of Old Faithful. (*b*) The relative frequency of eruption. All data are for 1979 (unpublished data provided by R. Hutchinson, U. S. National Park Service, from analysis of 3308 eruptions).

The maximum length of the water column in the immediate reservoir prior to an eruption is therefore about 16 m.

For nearly a century after its discovery, Old Faithful maintained a fairly regular pattern of eruptions, with intervals between eruptions averaging 60–65 min. During most years, Old Faithful exhibited two types of eruptions: "shorts," which were 2.5–3.5 min in duration, and "longs," which were about 5 min in duration. During the 1970s the length of the repose interval, I, following an eruption was quite closely related to the duration of the eruption, D. The empirical formula

$$I = 10D + 30 \tag{17}$$

(I and D in minutes) proved very useful to the National Park Service for predicting when eruptions would occur.

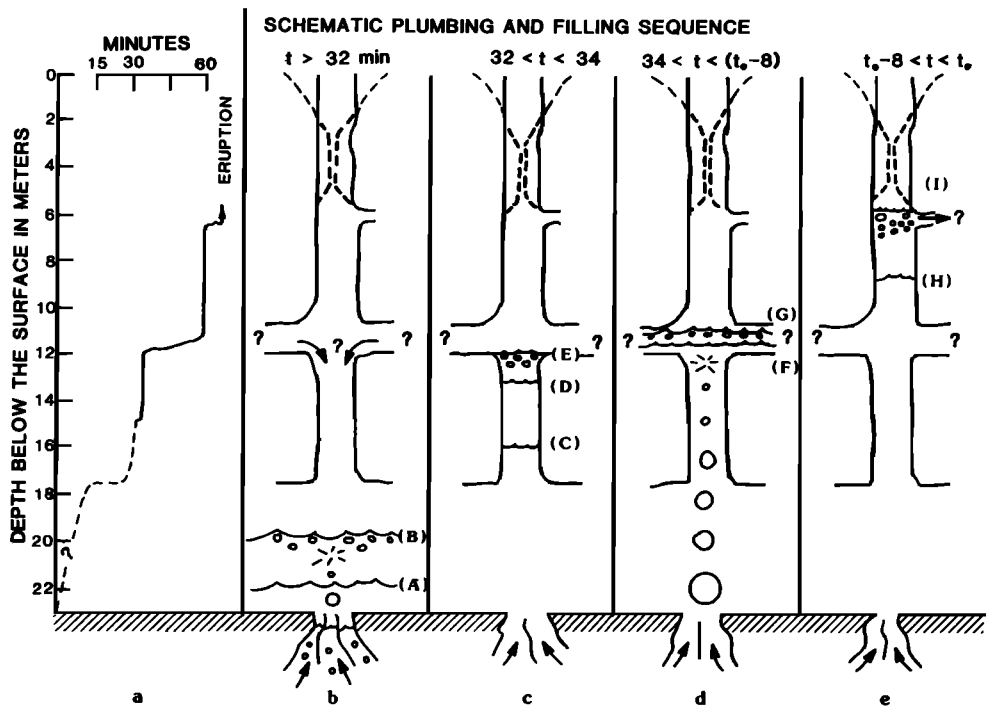

Figure 17. (*a*) Rate of filling of Old Faithful, as inferred from reported float measurements in 1948 [*Birch and Kennedy*, 1972]. Time $t = 0$ was taken when the probe was lowered. Recent (unpublished) work by the author and J. Westphal shows differences in details of the filling rate but does not change the general discussion chosen for this paper. (*b*)–(*d*) Schematic diagrams of the conduit of Old Faithful. The solid line represents the width versus depth in the widest direction (approximately east-west), and the dashed line represents estimated narrowest dimensions. The filling rate shown is based on the float measurements in Figure 17*a* and an assumption of constant recharge rate. Time until the next eruption is indicated at the top.

In the past few years the duration-interval behavior has changed dramatically, although changes in the observable characteristics of the geyser during an eruption (such as height versus time) have not been apparent. Intervals averaged over a month commonly exceed 75 min, and individual intervals have sometimes exceeded 100 min. The interval-duration equation no longer applies to the same statistical accuracy; in 1987, short eruptions ceased for a while, and only long eruptions occurred (R. Hutchinson, National Park Service, private communication, 1987). The mysteries of geyser eruptions have long intrigued scientists (the original theory of the inner workings of geysers was published by Bunsen in 1846), but questions about the inner workings of Old Faithful have taken on a new urgency because of these dramatic changes in behavior.

The Recharge Process: Clues to Geothermal Seismicity

After an eruption ceases, the conduit is empty (or nearly so) and must be recharged with both water and heat. Estimates of total volume erupted and conduit dimensions give an approximate recharge rate of 6 kg/s (liquid water) [*Kieffer*, 1984*a*, p. 66]. A working model for recharge of fluids and heat to the geyser is based on measurements of depth and temperature versus time by *Birch and Kennedy* [1972]. Water rises slowly up the conduit during the recharge interval, as shown by the levels A–I in Figures 17*b*–17*e*. During the rise, temperatures range from 93°C at the surface to 116°–118°C at the bottom of the immediate reservoir. The temperature at any depth fluctuates with time, as can be seen, for example, by examining the temperature-depth-time curves in Figure 18; note especially the temperature behavior at 18 m depth during the period 35–25 min before the eruption. However, the overall effect is a general heating of the water relative to the reference boiling curve, shown on each temperature-depth curve in the sequence in Figure 18. The hottest water at the bottom is about 7°–9°C below the boiling temperature for the total pressure at the bottom, ~0.23 MPa (2.3 bars) (0.08 MPa (0.8 bar) atmospheric pressure plus 0.14 MPa (1.4 bars) hydrostatic pressure). Because the deep water is hotter than the shallow water, heat for the recharge cycle is most likely supplied by the addition of hot water or steam at the base of the immediate reservoir,

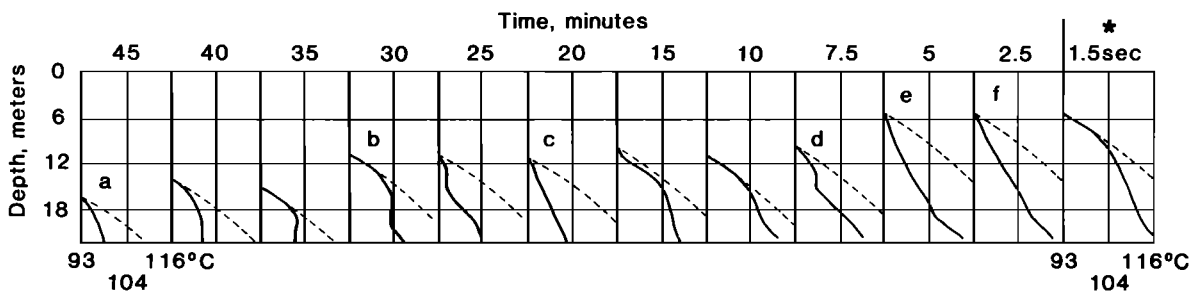

Figure 18. Relations between seismic events, level of filling, and temperature in the conduit of Old Faithful. (Top) Data on depth of water in the conduit at various times (graphs above the histogram) versus the temperature of the water and versus the reference boiling curve (the top curve in each small graph). (Bottom) A histogram of the number of seismic events per minute through a recharge interval at Old Faithful. Letters a–f show approximate correlations between temperature-depth curves and the histogram.

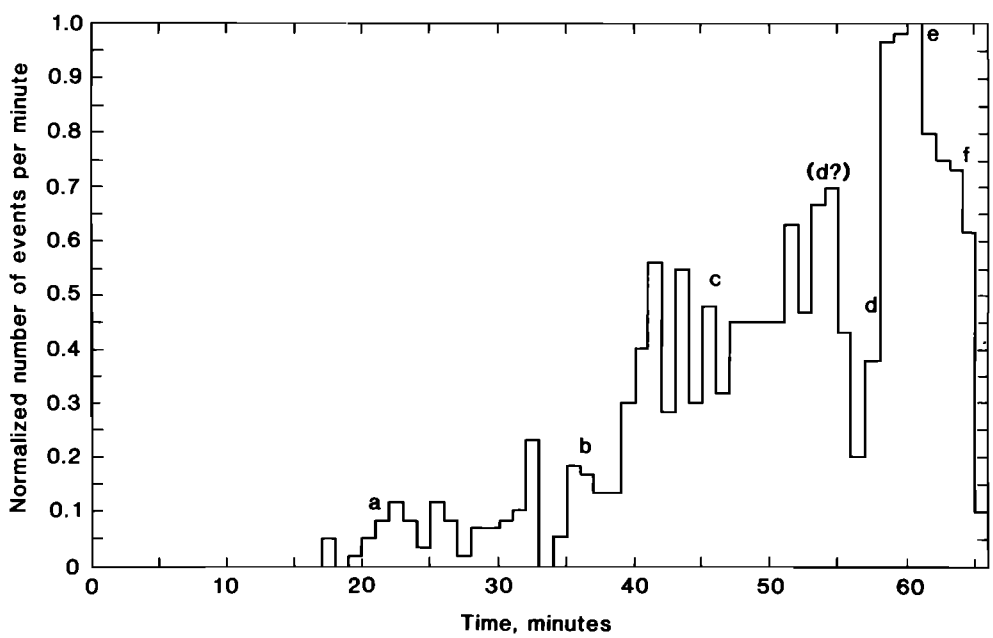

indicated by flow arrows and bubbles at the bottom of Figures 17*b*–17*e*.

Two processes probably contribute to the mixing of the hot, deep water with the cooler surface water: convection and migration of steam bubbles, illustrated schematically in Figures 17*b* and 17*d*. It is not clear that the two processes can be distinguished by using available measurements. Much of the deeper water is too cool to boil under the total pressure at any given time (Figure 18). However, since the temperature of the deeper water exceeds the atmospheric boiling temperature of 93°C, this water is superheated relative to the boiling point at atmospheric pressure. If such superheated water is convected upward, steam bubbles form if the pressure decreases below the saturation pressure of the water. For example, 3% of the deep water at 116°C will transform to steam when the total pressure decreases to 0.1 MPa (1.0 bar). As steam bubbles rise, however, they encounter cooler water and may collapse (shown schematically by the asterisk in Figures 17*b* and 17*d*). Although this process cannot be directly observed in the depths of Old Faithful, it is easily observed in a pot on a stove, as well as in other geysers, such as Strökker in Iceland, where the steam bubbles rise into a diverging surface pool and can be observed both to collapse before reaching the surface and to reach the surface and explode into a beautiful fragmenting shell (Figure 19). In geysers where the bubbles can be directly observed, they frequently occupy the full diameter of the conduit, which may be of the order of, or more than, 1 m.

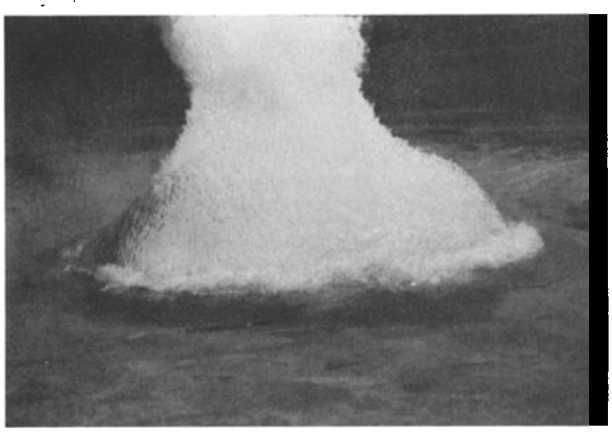

Figure 19. Bubble erupting from the vent of Strökker geyser, Iceland, through a surface pool of water. Bubble diameter is about 2 m. Note fine-scale structure on bubble surface. (Photograph by H. Kieffer.)

Collapse of the bubbles, and release of their latent heat, is probably a major process by which heat is transferred upward in the water column [*White*, 1967], and the collapse of these bubbles is believed to cause the individual seismic events observed.

The number of seismic events per minute an be crudely correlated to the temperature-depth-time evolution of the water in the conduit (Figure 18); the accuracy of this correlation is not great because the seismic data and the temperature data were obtained 40 years apart (see *Kieffer* [1984*a*] for details). In Figure 18 the initial time ($t = 0$) for the histogram of seismic events shown was taken at the beginning of an eruption that was about 4.5 min long. A 66-min interval followed before the next eruption. The first appreciable seismicity started at about 21 min (that is, 45 min before the next eruption), and the associated temperature-depth conditions are indicated by the frame on the left of the top line at 45 min and by the data at the two letters "a." Successive graphs in this figure labeled with decreasing times (40, 35, 30 min, . . ., down to 15 s) show the gradual filling and heating of the geyser and the correlations with seismic details. The cause of the seismicity will be summarized in this paper, but an equally fascinating problem is the cause of the two periods of seismic quiet that occur 1 min and about 10 min prior to the eruption (see *Kieffer* [1984*a*] for theory regarding this phenomenon that precedes all eruptions).

The collapse of a vapor bubble in a liquid of its own composition can occur within milliseconds [*Fujikawa and Akamatsu*, 1978, 1979] and pressures in the collapsing cavity can be as large as a few to tens of megapascals (tens to hundreds of bars) [*Fujikawa and Akamatsu*, 1978; *Biasi et al.*, 1972]. The high pressures generated by the bubble collapse decay quickly with distance, becoming seismic-level disturbances at distances of only a few bubble radii.

The acoustic noise of collapsing steam bubbles can be detected by seismometers placed around Old Faithful (Figures 15*a* and 20). The seismic codas of two eruptions, labeled A and B, are shown in Figure 20. These codas are primarily due to water falling back from the top of the erupting column onto the ground (this fallback was just beginning to occur when Figure 14 was taken; it is visible on the right side of the photograph). Short, discrete bursts of seismicity occur throughout most of the recharge interval (four such events, indicated in Figure 20, are shown enlarged in Figure 21). The number of seismic events per minute increases as the geyser fills and the fluid becomes generally hotter (Figure 18, histogram).

Two characteristics of this seismicity are the relatively high frequency content of the individual events (a few tens of hertz) and the characteristic damping time of a few tenths of a second. The envelope of these signals is remarkably similar in shape to results obtained by *Hentschel* [1979, 1980] in laboratory experiments on collapsing bubbles, although the geyser signals are much longer in duration (tenths of seconds compared with hundreds of microseconds), presumably because of the much larger size of the geyser bubbles.

A collapsing bubble could cause the observed seismicity by generating waves within the fluid column, as illustrated in Figures 22*a* and 22*b*. These waves set the fluid in the conduit into resonance; that is, the conduit is an organ pipe filled with liquid water and is set into resonance

by the occasional (or frequent) collapse of a large steam bubble. Detailed treatment of the disturbance caused by a single bubble as a hydraulic transient [*Kieffer*, 1984*a*] accounts for the distensibility (approximately the elasticity) of the conduit walls and allows the damping of the signals to be calculated.

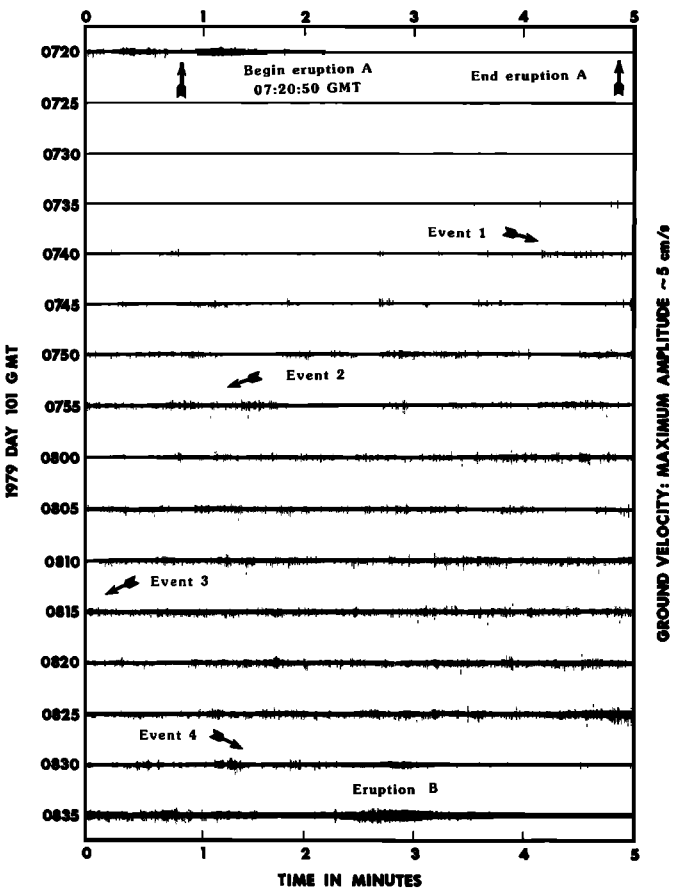

Figure 20. A seismic record of one eruption cycle of Old Faithful. Details of the seismic events labeled 1–4 are shown in Figure 21. To obtain the histogram of Figure 18, the number of these events exceeding a peak-to-peak amplitude of 4 cm/s were counted.

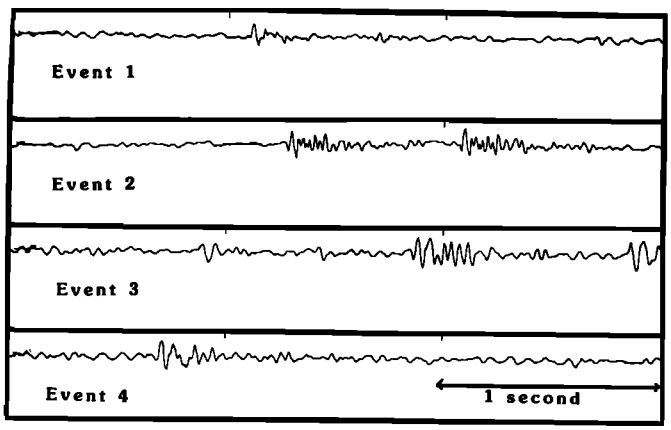

Figure 21. Details of the four impulsive seismic events from Old Faithful Geyser as indicated in Figure 20. Note that the dominant frequencies range from ~20 to ~40 Hz.

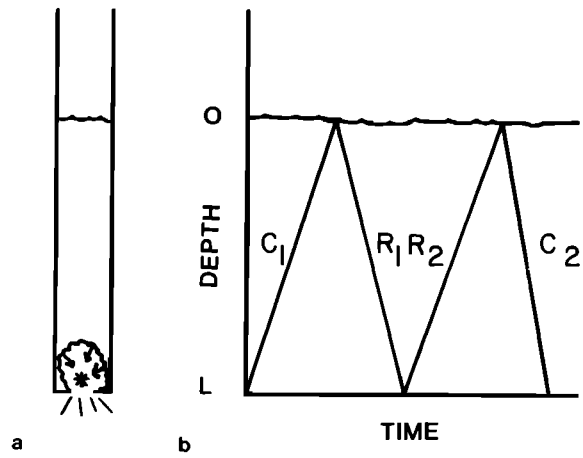

Figure 22. Schematic drawing of waves propagating in a standing column of water of depth L. (*a*) The collapse of a steam bubble (asterisk) in the base of the column. (*b*) One cycle of compression (C) and rarefaction (R) waves due to bubble collapse in the bottom of the conduit.

Even in a fissurelike pipe with the irregular shape of Old Faithful, the characteristic fundamental frequency of oscillation induced should be close to the longitudinal resonance of a cylindrical pipe. The geometry of the conduit determines whether the conduit should be considered open-ended or closed-ended. Even though the conduit may flare with depth, the bottom seems relatively well defined, and so, in the absence of other data, the conduit is herein treated as a closed pipe with resonant frequencies given by

$$f = a/4L \tag{18}$$

where L is the length of the fluid column in the conduit. In this equation the sound speed a is the effective sound speed of the fluid modified for the distensibility of the conduit walls. The resonant frequency for an open pipe would be twice this value. Whereas a is 1440 m/s for pure water, it decreases to 1385 m/s if the distensibility of the walls of the conduit is accounted for.

The length of the fluid column in the conduit, L, depends on the time in the recharge cycle (note in Figures 17 and 18 how slowly the recharge process occurs): L is estimated to be 8 m when the seismicity is first detected and 16 m when the conduit is full near the time of an eruption (Figures 17*c*–17*e* and Figure 18). The corresponding resonant frequencies obtained from (18) are 43 and 20 Hz, values that approximately span the range of measured frequencies during the recharge interval (Figure 21). From hydraulic transient theory the characteristic damping time is 0.12–0.46 s, in good agreement with the duration of the observed pulses (Figure 21).

The resonant frequency associated with individual seismic events, and the duration of each event during the pre-eruption seismicity at Old Faithful, can be explained,

to first order, as arising from hydraulic transients in a slowly recharging column of liquid water. If the fluid in the conduit were, for example, a boiling, two-phase mixture, the sound speed would be dramatically lower, and the observed seismicity could not be explained so simply as arising from resonances of the liquid column standing in the immediate reservoir. In the next section I describe the transformation of the recharged liquid in the conduit as an eruption occurs and show how the associated change in sound speed of the fluid influences the resonant frequencies of the conduit during eruption.

Eruption Dynamics and Thermodynamics

An "eruption cycle" of Old Faithful consists of one eruption and one recharge interval. By convention, the start of an eruption cycle is taken as the onset of an eruption, although the first part of an eruption actually begins below ground level and cannot be monitored (see the discussion of preplay below). The visible flow field and its variation with time during an eruption are collectively referred to as the "play" of the geyser. The play consists of four parts which can be distinguished on a graph showing height of the eruption column versus time (Figure 23).

The first part of an eruption (the part that begins underground and fails to maintain a height above the surface of the ground for more than a few seconds) is "preplay," the ejection of water intermittently prior to the actual eruption (the last few episodes of preplay before the eruption, from −15 s to 0 s, are shown in Figure 23). Episodes of preplay last for a few seconds, and water is thrown to a height of a few meters or occasionally a few tens of meters. During preplay, water ejected upward into the atmosphere is cooled by expansion and entrainment. When this cooled water falls back into the conduit, it mixes with the heated conduit fluid. The resulting overall cooling of near-surface water can delay the onset of an eruption until the fluid has been reheated to initiation conditions.

The second stage of the eruption is called herein "initiation and unsteady flow." During this stage, the eruption column develops and rises in a series of bursts (typically one to eight) to a maximum height of about 30–50 m. This part of the eruption is typically 20–40 s long. Two minor bursts and four major ones occurred during the first 20 s of the eruption documented in Figure 23.

The third stage of the eruption, "steady flow," is an interval of about 30 s during which the column stays near maximum height. During this time, surges are observed in the eruption column at a frequency of about 2 Hz in short eruptions and 1–1.5 Hz in long eruptions (Figure 24*b*). The surges are shown photographically in Figure 14 and graphically from 20 to 45 s of the eruption documented in Figure 23.

The fourth stage of an eruption, the "decline," begins rather dramatically, after approximately 30 s of steady flow, with a drop in column height. The decline can last up to 3 or even 4 min; during this time the height of the column drops to about 10 m, and play continues at low levels.

Differences between long and short eruptions are threefold: the frequency of surging during the steady flow stage, the duration of the decline stage, and the seismic pattern following the eruption. Analysis of height-time data (such as those shown in Figure 23) for many eruptions reveals that there is no correlation of maximum height obtained, duration of maximum height, or number of bursts in the initiation stage with eruption duration (Figure 24*a*). The only measurable differences in eruption play between long and short eruptions are the frequency of the surges (Figure 24*b*) and the duration of the decline phase, which is simply truncated at about 2–3 min for a short eruption. Seismically, a period of about 20 min of quiet follows a long eruption (Figure 20), whereas seismicity begins immediately after a short eruption. After short eruptions we are able to hear water splashing in the bottom of the immediate reservoir, which suggests that it is not completely emptied during short eruptions and that the seismicity arises within the immediate reservoir.

Water near the surface of the recharging column boils nearly continuously, and vigorous boiling can accelerate

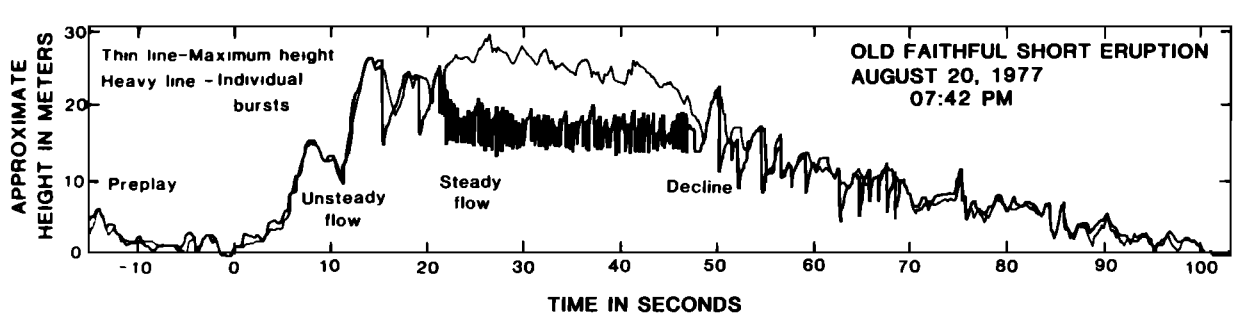

Figure 23. Height versus time for a short eruption of Old Faithful. The light line is the height of the water-stream column; the heavier line traces individual pulses of water, visible in Figure 14, in order to obtain the frequency of surging (approximately 1–2 Hz).

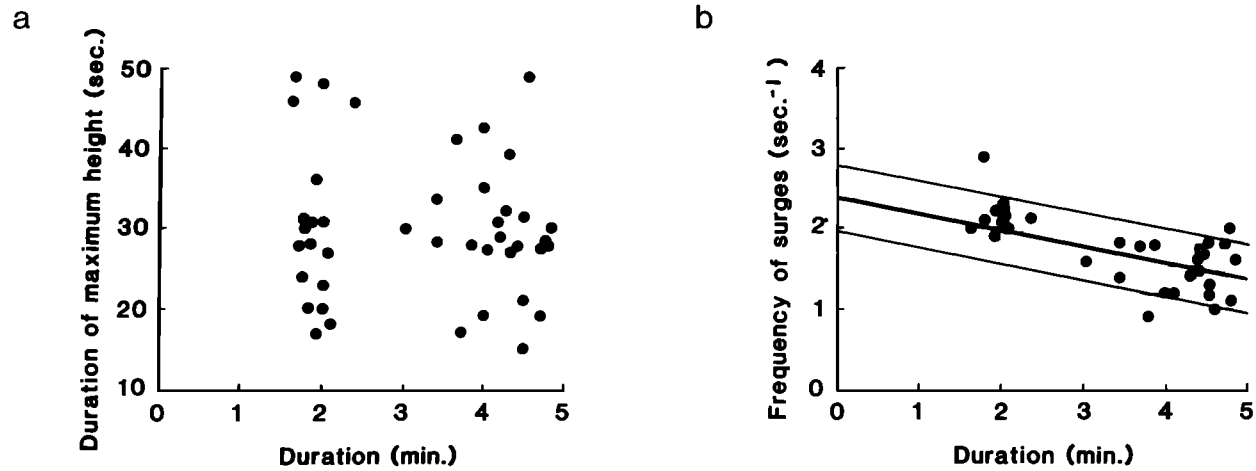

Figure 24. (*a*) Duration of steady flow stage (maximum height) versus duration of eruption of Old Faithful geyser, showing no correlation. (*b*) Frequency of surges versus duration of eruption showing inverse correlation.

fluid several meters upward. Early in the recharge cycle, the fluid is too deep in the conduit for vigorously boiled water to be ejected over the rim. Thus even though vigorous boiling and splashing occur within the conduit, the pressure distribution at depth remains unchanged because fluid is not removed from the conduit and an eruption cannot begin. An eruption therefore begins when two criteria are met: (1) the water must have risen high enough in the conduit so that vigorous boiling can discharge some water over the rim, thereby reducing the hydrostatic pressure on the fluid by removal of some mass (such ejection can occur when the fluid is within about 6 m of the top of the conduit) and (2) the underlying water must be hot enough so that the mass unloading triggers a positive feedback process.

A simplified diagram of Old Faithful modeled as a layered shock tube is shown in Figure 25. In the example shown I have arbitrarily divided the fluid in the column into seven cells of different length. Cell A has pressure-temperature conditions that follow the reference boiling curve. I chose the length of 1 m for this zone somewhat arbitrarily after watching the onset of about 200 eruptions

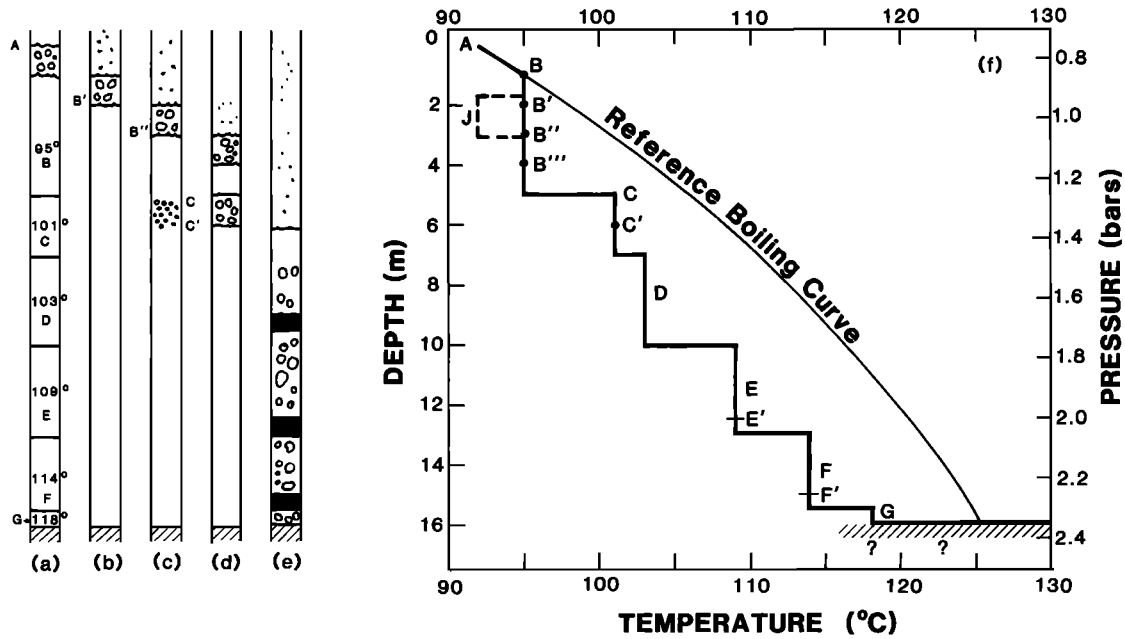

Figure 25. Old Faithful modeled as a shock tube. The initial configuration (Figure 25*a*) shows layers of fluid at different initial pressures and temperatures in their position relative to the reference boiling curve in Figure 25*f*. In Figures 25*a* and 25*f* the initial temperature is assumed constant within six convection cells (labeled B, C, D, E, F, and G). The fluid in cell A is assumed to be at pressure-temperature conditions on the boiling curve in order to trigger the eruption. Figures 25*a*–25*e* show five states in the unsteady unloading process of an eruption of Old Faithful. The segments shown with large "bubbles" are boiling; the segments shown as a fine "mist" are erupting from the conduit; and the three segments shaded black are liquid H_2O because of the relations of parts of cells D, E, and F to the reference boiling curve during the unloading process. The thermodynamic path of the unloading process is discussed in the text.

and estimating the amount of water ejected. Cells B, C, D, E, F, and G are each assigned different, but uniform, temperatures; they might be thought of as simplified convection cells. The overall temperature distribution of the cells mimics the temperature curve measured by *Birch and Kennedy* [1972] at 15 s before the onset of an eruption (see Figure 18, last temperature-depth graph). The top zone, A, 1 m in length, has been assumed to be the mass of water that is ejected out of the conduit to start the eruption (Figure 25*a*).

When A is ejected out of the conduit, the pressure on the underlying water is everywhere reduced by the weight of the ejected fluid (assume this to be about 0.1 bar; SI units are abandoned temporarily here for ease in following Figure 25). Relative to the reference boiling curve, therefore, the initial temperature distribution curve is elevated toward the boiling curve by 0.1 bar. If it is assumed that no large-scale temperature inversion exists, such as J (Figure 25*f*), some underlying water is now superheated with respect to the boiling temperature at the new pressure, specifically, any water that was originally within 0.1 bar of the reference boiling curve. In the example shown, the water between B and B′ will boil (Figure 25*b*). When this water is erupted, more underlying water will boil: any water that was originally within 0.2 bar of the reference boiling curve. In Figure 25 this is only the water between B′ and B″, although the water at the top of cell C is now very close to the reference boiling curve (Figure 25*c*). When this water has been unloaded, the pressure is everywhere 0.3 bar less than the initial pressure, and water between B″ and B‴, as well as between C and C′, will boil. Note that because of the weight of B″–B‴, the fluid between B‴ and C cannot boil until some of the fluid in B″–B‴ erupts from the conduit. Presumably, as the water between B″ and B‴ erupts, and as C–C′ boils and expands, the liquid water between B‴ and C will be pushed up and will boil as the pressure decreases. Slugs of liquid water trapped between slugs of boiling froth should be expected because of the different possible relations of the fluid temperature to the reference boiling curve (Figures 25*c*–25*e*).

When fluid has been erupted down to level C′, 6 m of water will have been ejected, and the pressure in the column will be everywhere 0.6 bar less than the initial pressure. Except for small amounts of fluid between E′ and F and between F′ and G (Figure 25*e*), the fluid will be everywhere on the reference boiling curve, and the conduit will become nearly completely filled with a two-phase mixture. The fluid is probably a boiling liquid at depth, grading upward into the steamy aerosol that emerges at the surface.

Further details of this unloading process are unknown; depending on the constriction, shock and rarefaction waves may play a prominent role in ejecting the different layers of water [*Kieffer*, 1984*a*], or choked flow may be more important in controlling the mass flux rate (see following discussion). Resolution of this question may only arise from detailed theoretical or laboratory modeling because of the extreme difficulty of field measurements of conduit geometry and time history of the fluid flow.

Because the initial pressure-temperature curve at the onset of an eruption lies no farther than 0.05–0.07 MPa (0.5–0.7 bar) below the reference boiling curve, the whole column of fluid in the conduit lies on the reference boiling curve after the unloading of only 5–7 m of the water. Thus when about half of the vertical length of the water column has been unloaded, the pre-eruption "organ pipe" filled with liquid water has been transformed into a steamy two-phase nozzle. (Note that if the conduit is perceived as a nozzle, the original standing water occupied only 16 m of length, whereas the erupting fluid fills the full 22 m and extends into a jet 30–50 m high outside the conduit.) It is likely that the "bursting" observed during the unsteady initiation of the eruption represents the eruption of progressively hotter parcels of water and that the transition from unsteady bursting flow to steady surging flow observed in the behavior of the eruption column (Figure 23) occurs when the whole immediate reservoir is filled with a two-phase fluid.

As the water in the base of the reservoir is decompressed to atmospheric pressure, some of the enthalpy stored in the hot fluid is converted to kinetic energy. The hottest water, at 116°C, has an enthalpy (relative to the triple point) of 486.72 kJ/kg and an entropy of 1.4842 kJ/kg K. If this fluid decompresses isentropically to 93°C, at 0.08 MPa (0.8 bar) pressure, 4 wt % of the liquid is converted to vapor. The final enthalpy of the mixture is 482.83 kJ/kg, so 3.89 kJ/kg is available for kinetic energy. This is sufficient energy to accelerate the fluid isentropically to a velocity of 88 m/s.

Although the velocity at the exit plane of the geyser has not been directly measured, the fact that the density of the erupted fluid is large compared with atmospheric density suggests that a simple ballistic calculation of velocity based on the height of the eruption column might be used to estimate ejection velocity. This calculation uses $x_m = u_0^2/2g$, where x_m is the maximum height, u_0 is the exit velocity, and g is the acceleration of gravity. For $x_m = 50$ m this equation yields $u_0 = 31$ m/s. If the acceleration is presumed to begin at the base of the conduit, x_m could be about 70 m, and u_0 from this model is 37 m/s.

However, because an eruption of Old Faithful produces a jet rather than a "ballistic billiard ball," the simple ballistic equation may not accurately estimate the exit velocity. Experimental data on the dynamics of negatively buoyant plumes [*Turner* 1966; *Chen and Rodi*, 1980] give

the relation

$$x_m = 1.85\, F^{1/2} D \tag{19}$$

where F is the densimetric Foude number:

$$F = u_0^2 \left[\frac{\rho_0}{(\rho_a - \rho_0) g D} \right] \tag{20}$$

In this equation, ρ_0 is the fluid density, ρ_a is the density of the fluid into which the jet is emerging, and D is the diameter of the jet, assumed axially symmetric. (This F is comparable to $(Fr)^2$, with Fr as defined in (15).) The absolute value of the density difference is used in (19), where the square root of F is needed. For the exit plane at Old Faithful (1.5 × 0.6 m fissure), take D = 1.1 m. Assume that ρ_0 = 11.23 kg/m^3 (4% vapor) and ρ_a = 0.7 kg/m^3. The above equations give u_0 = 78 m/s, a value in surprisingly good agreement with the velocity of 88 m/s predicted simply from the enthalpy change of the fluid. The difference may be within the uncertainties of the field measurements or may suggest that the enthalpy conversion is roughly 90% efficient.

The low-frequency surging (~1–2 Hz) observed when the geyser is in steady flow (Figures 14, 23, and 24) could be the resonances of the conduit filled with the two-phase mixture. The equilibrium sound speed of an H_2O mixture composed of 4% vapor is 57 m/s at 1 bar pressure. The sound speed does not vary significantly between 0.8 bar atmospheric pressure and 0.18 MPa (1.8 bars) vapor pressure for the fluid boiling at 116°C at the bottom of the vent. The sound speed would decrease dramatically, however, in the zone where the vapor fraction approaches zero (that is, right in the region where bubbles begin to nucleate in the liquid water phase), as shown in Figure 3, vertical line (a). However, I assume that the vertical range over which the sound speed is substantially lower than 50 m/s is small and that the sound speed of 57 m/s is typical of the fluid in most of the conduit. The resonant frequency of a 22-m closed pipe with this sound speed would be 0.64 Hz, corresponding to a period of 1.5 s. Although this frequency is about a factor of 2 lower than that measured for along eruption (1–1.5 Hz), it is certainly correct in order of magnitude and indicates the dramatic change in resonant frequencies as the fluid goes from a single-phase liquid to a two-phase mixture. Given the uncertainties in the model (the relatively unknown geometry of the conduit and whether or not it is best approximated as an open- or closed-ended pipe) and the extreme difficulty of measuring each individual eruption surge, the calculated and measured frequencies are probably in satisfactory agreement.

Because we have no reason to believe that the sound speed of the fluid is any different in long versus short eruptions, the change in surge frequency with eruption duration can be interpreted as representing an effective change in the length L of the resonating column. The possibility that multiple chambers containing fluid exist cannot be excluded, and emptying of different numbers of such chambers could account for an effective change of L. Another possibility is that water is vaporized to different levels in the eruptions of differing durations. During a long eruption, for example, all water in the immediate reservoir is converted into a two-phase mixture, and the immediate reservoir is completely emptied. For the long eruptions the bottom of the conduit is probably truly the geyserite bottom reached by probe, and L is the measured 22 m. During a short eruption, only part of the water in the immediate reservoir appears to be discharged. There is therefore probably a level below which water does not vaporize during short eruptions. In these eruptions the surface of the unvaporized water would be the "effective bottom" of the reservoir because of the large difference in acoustic impedance between boiling and liquid water; that is, the length L would not be the physical conduit length but a shorter value equal to the length of water column vaporized. This could account for the higher surge frequencies observed during short eruptions (Figure 24*b*). The mechanism whereby the water, which is initially at 116°C when an eruption begins, is prevented from vaporizing under pressure reduction remains a mystery. The most common speculation is that cold water can occasionally enter the reservoir during an eruption, but there is no proof of this, and it is perhaps equally plausible that local temperature inversions in the fluid could quench eruptions.

Speculations and Summary

Is the flow from Old Faithful choked? Is there supersonic flow anywhere in the eruption jet? There are too few data to permit firm conclusions. A few speculations can be offered, although calculation of choking conditions in two-phase flow is a notoriously difficult problem even in well-designed pipes [*Wallis*, 1969, and references therein].

The highest vapor pressures in the reservoir will be generated as the hottest water boils: 0.175 MPa (1.75 bars) as the 116°C water boils. Equilibrium expansion to atmospheric pressure of 0.08 MPa (0.8 bar) produces a fluid that is about 4% vapor. Given a maximum reservoir pressure of 0.175 MPa (1.75 bars), the choke pressure can be calculated to be about 0.13 MPa (1.3 bars) [*Moody*, 1965]. Experimental evidence [*Fauske*, 1962] suggests that this calculated choke pressure is too high and that the choke pressure could be as low as about 0.55 of the reservoir pressure, about 0.09 MPa (0.9 bar). The near similarity of atmospheric pressure and estimated choke pressure suggests that the flow could be choked when this

hottest water is flowing but that supersonic flow in the diverging part of the conduit will be weak. The discussion above about the decompression process suggests that choked flow would be most likely during the steady-flow stage, beginning 20–30 s into the eruption.

Assume that choking occurs at conditions very close to those seen at the exit plane, that is, at 0.1 MPa (1 bar) pressure when the fluid is about 3% vapor. The mass flux $\dot{m}$ is given by

$$\dot{m} = p^* A^* a^* \tag{21}$$

where A^* is the area of the choke plane and a^* is the sound speed, 45 m/s for equilibrium at 0.1 bar pressure. The density ρ^* of the fluid is 19.68 kg/m^3 (3% vapor), and the choke area is about 0.15 m^2. The calculated total mass flux is 132 kg/s. Of this, 96%, or 127 kg/s, is liquid water. This value is satisfactorily close to the measured value of water in the runoff channels from Old Faithful (114 kg/s), given the extreme difficulty of measuring the discharge accurately and the relatively large uncertainty of the choke area A^*.

If, as calculated above, the exit plane velocity is ~80 m/s and the equilibrium sound speed at the exit plane is 57 m/s, the implied Mach number at the exit plane is ~1.5, barely supersonic within the uncertainties of the modeling. It is therefore not surprising that shock features such as Prandtl-Meyer expansion, visible shock waves, or noise originating from shocks within the plume are not observed at Old Faithful. In contrast, Beehive geyser (Figure 26*a*), which sits just a few hundred yards from Old Faithful and erupts too erratically to be easily monitored, sounds like a jet engine and, with a little imagination, can be envisioned to contain internal shock waves (the arrow in Figure 26*a* points to three diamond-shaped structures that may be shock waves). These shocks are similar to those observed at weakly supersonic geothermal well heads (Figure 26*b*).

In summary, Old Faithful is a complex two-phase nozzle, possibly sonic or weakly supersonic, and certainly large enough in scale for both gravity and compressibility to be important. Although available data still do not permit a detailed model for the eruption dynamics, they have served to point out new directions for experiments and observations, some of which are now in progress. One of the most important directions of research focused on by these discoveries relates to the similarities in seismicity between geysers and volcanoes that exhibit harmonic tremor (Figure 15). Harmonic tremor has for decades been attributed to magma motion and/or fracture propagation in volcanoes, but the quantitative nature of the mechanism causing it has been elusive. The geyser study suggests that bubbles in groundwater contained in fissures or pockets surrounding hot magma could be the source of tremor in some settings [*Kieffer*, 1984*a*], and quantitative studies of this mechanism are now in progress [*Leet*, 1988]. Because we know neither the dimensions of the conduits containing the fluid nor the nature of the fluid that is causing the seismicity at volcanoes, this is a very difficult problem. The study of Old Faithful, where at least constraints can be put on the fluid and on the conduit dimensions, is thus

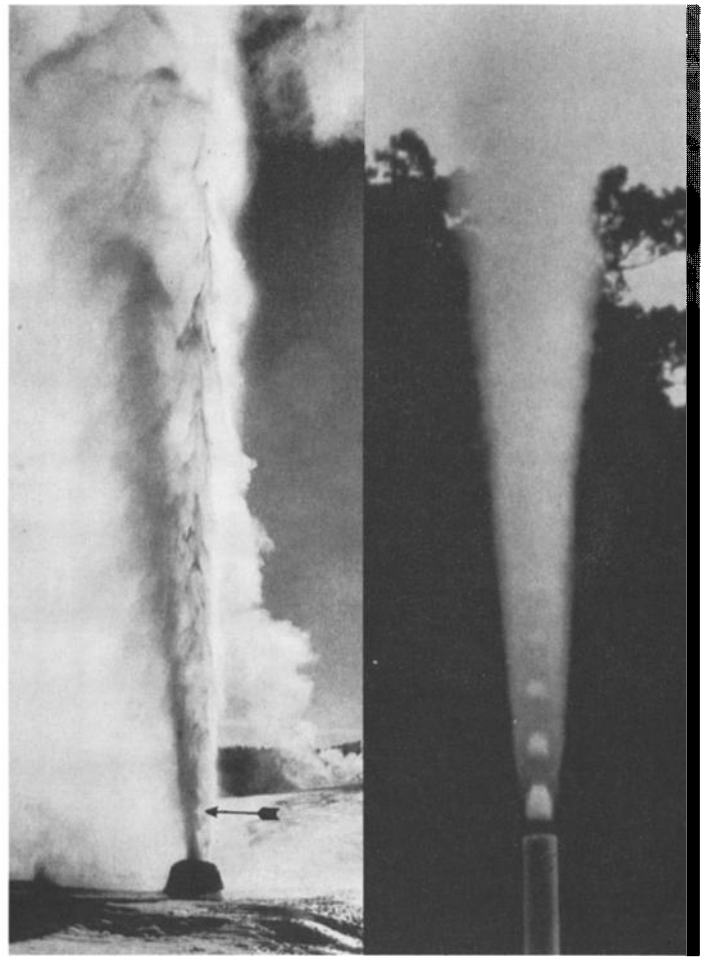

a b

Figure 26. (*a*) Beehive geyser in eruption. The cone is about 1 m high. The arrow points toward the second of three white diamonds in the center of the flow, interpreted as shock wave structures within supersonic flow. In the background a low cloud of steam marks the vent of Old Faithful, and the column of steam ascending toward the left of this area, behind the plume from Beehive, is probably from an eruption of Old Faithful that had just ended when this photograph was taken. Although no physical connection between Old Faithful and Beehive (which are separated by the Firehole River) has been proven, their eruptions are sometimes coupled. (Photograph by J. Schmidt [see *Fuller and Schmidt*, 1984], reprinted with permission.) (*b*) Geothermal well MG-5, Tongonan, Philippines, showing diamond shocks that can be compared with those in Beehive geyser (Figure 26*a*). (Photograph by C. Darby, KRTA Ltd., Auckland, New Zealand.)

Figure 27. A geyserlike eruption of Mount St. Helens, April 1, 1980. An ash-laden density flow rolls down the southwestern slopes (on the right) from the summit crater at about 2930-m elevation, while steam separates and rises to ~4500 m. (Photograph by H. and S. Kieffer.)

relatively unique. Fluids proposed for the source of volcanic tremor (undersaturated magma, gassy magma, water) can have sound speeds that differ by nearly three orders of magnitude, and the above discussion suggests that there will be an ambiguity in decoupling the effects of conduit dimensions from fluid properties in any analysis of volcanic harmonic tremor. This is an active area of research in volcanology because of the regular occurrence of volcanic tremor at some volcanoes near heavily populated areas where forecasting has enormous implications for life and economy; for example, at Ruiz volcano in Colombia, some seismicity strongly resembled that of Karkar volcano (Figure 15) and has now been interpreted to indicate underground geysering and phreatic activity (as summarized by *Williams and Meyer* [1988]). Laboratory studies of the dynamics of large collapsing bubbles and of two-phase flow in long pipes of variable area are needed. In particular, theoretical and experimental work on the dynamics of compressible flow with gravitational effects will be required to deal with problems involving these fluids at geologic scales.

6. MOUNT ST. HELENS: A SUPERSONIC JET

Geologic Setting

Mount St. Helens became famous as an "active volcano" on May 18, 1980. However, that eruption was heralded by nearly 6 weeks of precursor activity during which eruptions were strikingly similar in scale, frequency, and fluid dynamics to eruptions of major geysers like Old Faithful. On March 27, 1980, after a repose of one century and ominous seismicity for a week, an unobserved eruption created a small crater in the summit of the mountain. For a few weeks, eruptions of steam and ash emanated from the summit (Figure 27). Studies of deformation of the mountain, and later events, strongly suggest that magma was being intruded into the edifice from depth at this time (Figures 28*a* and 28*b*). Water near the magma was heated and convected upward (indicated by arrows in Figure 28*a*), emerging in eruptions that were geyserlike in scale (hundreds of meters to a few kilometers high), duration (minutes to tens of minutes), and frequency (every few hours). The repeated eruptions created and enlarged a conduit and summit crater. Crushed rock, ice, ash, and water were intermittently ejected. Some of this material fell back into the conduit and clogged it temporarily, only to be reworked and ejected in successive eruptions. These early eruptions were driven by heated ground water: no magma was involved.

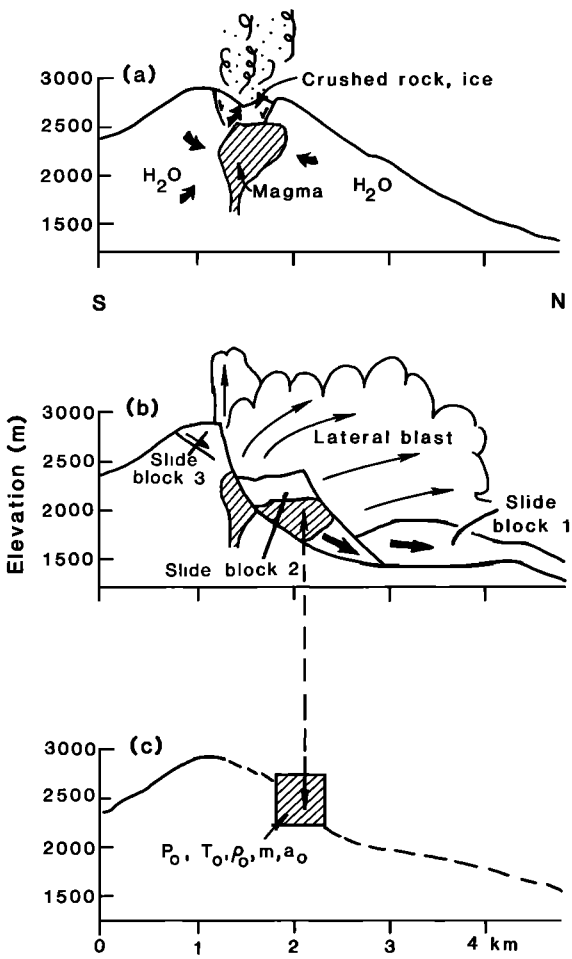

Figure 28. (*a*) South-to-north cross section showing schematically the conditions inside Mount St. Helens during March, April, and early May 1980. Magma has moved high into the mountain. (*b*) Reconstruction [*Moore and Albee,* 1981] of the initiation of the lateral blast on May 18. (*c*) Schematic drawing of initial conditions assumed for the fluid flow model. Symbols P_0, T_0, ρ_0, m, and a_0 are discussed in text.

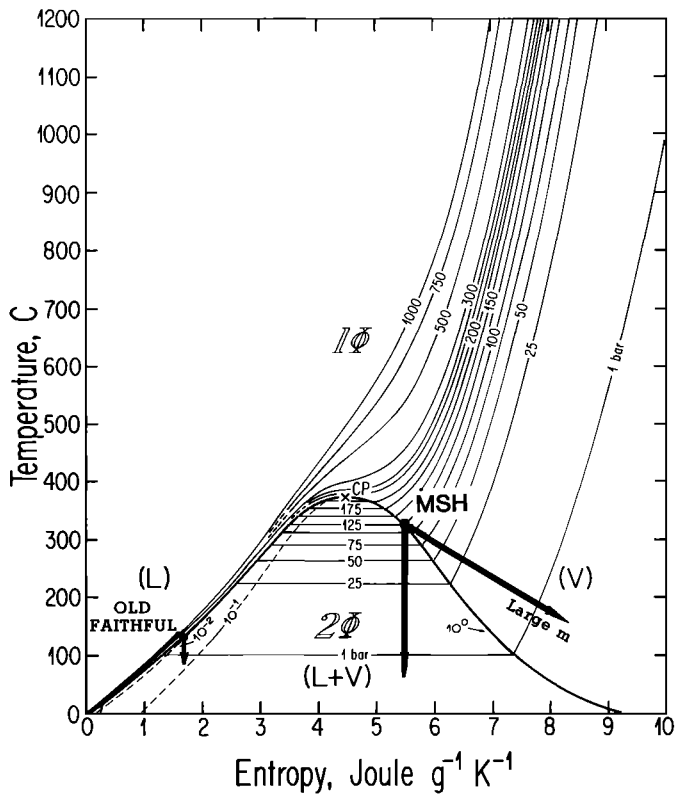

Figure 29. Temperature-entropy diagram for H_2O with isobars (solid lines except where closely spaced) and isopleths (dashed lines inside two-phase field). Symbols 1Φ, 2Φ, *L*, and *V* are the same as in Figure 3. CP, critical point. On the left, an isentrope for an eruption of Old Faithful; on the right, two isentropes for eruptions from the assumed Mount St. Helens (MSH) initial conditions.

Although these eruptions were more geyserlike than "volcanic,"they differed thermodynamically from eruptions of most geysers because the erupting vapor carried a heavy load of particulate material, crushed rock and ice gouged from the conduit and crater (this particulate material gives the lower part of the eruption plume in Figure 27 a dark color). The mass loading by this material affected the thermodynamics in two ways: the entrainment of solid fragments increased the bulk density of the fluid, and heat transfer between the solids and the expanding gas altered the expansion of the gas from that which would be obtained by a two-phase mixture or vapor alone. The mass loading of these eruptions was probably relatively light, especially in the dusty steam (Figure 27), and thus the pseudogas approximation discussed in section 3 might be a rather good description of these fluids. In such a model, mass loading is taken into account as an increased molecular weight of the mixture (see the equations at the top of Figure 4). Heat transfer from hot particles to cooler vapor is accounted for by a decrease in the isentropic exponent of the perfect-gas law.

The expansion of a mass-loaded vapor is contrasted with the expansion of a vapor alone, or of a decompressing liquid, in Figure 29. On the left side of this figure an isentrope representing decompression from the hottest water of Old Faithful (116°C) to 93°C is shown (refer to discussion in previous section). On the right side, two isentropes for hotter conditions more appropriate to the volcanic environment of Mount St. Helens are shown (labeled MSH). The particular initial conditions picked are discussed below as lateral blast conditions, but the thermodynamic point to be illustrated here is the qualitative difference between the two isentropes. The vertical line under the MSH label is an isentrope of pure steam. Note that isentropic expansion results in condensation of a liquid fraction. In contrast, the isentrope slanted toward the lower right, and labeled "large *m*" is the isentrope of the vapor phase in a mixture that contains sufficient mass loading *m* that heat transfer between the particles and gas is effective. The heat transfer increases the entropy of the steam phase throughout the expansion, and condensation is thereby prevented. As can be seen from this figure, under some circumstances, mass loading can simplify the fluid

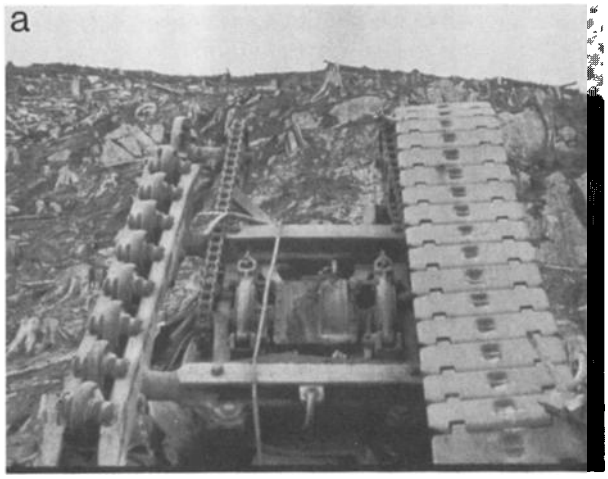

Figure 30. (*a*) Damage to heavy logging equipment during the May 18 lateral blast. (*b*) Damage to trees. (Photographs by H. and S. Kieffer.)

dynamics by preventing phase changes: the entropy of a gas phase is increased by heat conducted from solids, and thus formation of a condensed phase is suppressed. However, complications of heat transfer, drag, and interparticle interactions arise. No theoretical models yet account for these effects realistically for the range of particle sizes, particle shapes, and mass loading typical of volcanic eruptions.

The north flank of Mount St. Helens was badly fractured and weakened by the intrusion of magma in March and April 1980. At 0832 on May 18 a magnitude 5.2 earthquake shook the mountain, and at least three large landslide blocks broke loose and slid downhill toward the North Fork of the Toutle River (Figure 28*b*). Within a few seconds the pressure on magma, hot water, and gases inside the mountain was greatly reduced, and their rapid expansion produced the devastating event that was to become known as the "lateral blast." Magma was present in each slide block, but the lateral blast appeared to originate most strongly from slide block 2. The evolution of this blast was recorded by several eyewitnesses, by seismic equipment stationed around the mountain, by weather barometers, and by damage to the environment and to man-made equipment around the mountain [*Lipman and Mullineaux*, 1981]. Nearly 600 km^2 of forest was devastated, and approximately 60 people were killed. Heavy logging equipment was tossed and overturned (Figure 30*a*). Trees were totally stripped from the land over a large area, and where they remained, as much as 10 cm of bark and wood was abraded, the interiors being impregnated with rock shrapnel (Figure 30*b*). The pattern of tree blowdown (Figure 31) provided a remarkable record of local flow directions, certainly a flow-field pattern to challenge geologists and fluid dynamicists for years to come.

Figure 31. Typical pattern of tree blowdown. Note that the tops of the trees and most of the small limbs are missing. The contrast in this photograph is low because volcanic ash mantled trees and slope when it was taken, shortly after May 18, 1980.

In the region closest to the volcano, trees were either stripped from the land or felled subradially away from the vent, and the blowdown direction showed little dependence on the terrain (Figure 32). This zone is called the "direct blast zone" to emphasize that the blast traveled directly away from the mountain without regard to even major topographic obstacles. Surrounding the direct blast zone is a zone in which topography did influence the blowdown direction, called the "channelized blast zone" to emphasize that the blast followed channels in the topography. Surrounding this region and marking the limits of the devastated area is the "singed zone," a zone in which trees were left standing but were singed by the heat of the blast as it became positively buoyant and lifted from the ground into the atmosphere [*Kieffer*, 1981*a*].

This devastation was caused by the eruption of more than 10^{14} g of magma, hot water, and entrained glacier ice and trees. The vent through which the material emerged covered a large fraction of the north side of the mountain. Available evidence allows many theories, and geologists do not even agree on initial and boundary conditions for the flow (see, for example, the contrasting models of *Kieffer* [1981*a*, *b*, 1984*b*], *Eichelberger and Hayes* [1982],

Malin and Sheridan [1982] and *Moore and Rice* [1984]. I describe below my model for the blast, a model that emphasizes the role of gas expansion and nozzle flow. Given a plausible set of simplifying assumptions, this model attempts to define the flow characteristics and to correlate these predicted characteristics with features in the devastated area: tree directions, the transition from direct to channelized blast zones, measured velocities and temperatures, and the general shape of the devastated area.

A Simple Nozzle Model

In my model the lateral blast is simplified to the problem of the eruption of a pseudogas from a single reservoir under pressure into an atmosphere at lower pressure (this simplification can be seen by comparing Figures 28*b* and 28*c*). The thermodynamic properties and reservoir geometry are also simplified accordingly (Figure 28*c*). The fluid is described by its initial (average) pressure P_0, temperature T_0, and mass ratio m of solid to vapor phases. The reservoir is assumed to have resembled a converging nozzle whose exit plane (vent) was the landslide scarp left on the north face of the mountain by the removal of the avalanche material. Although the time history of evolution of the landslides was complex, for modeling purposes the triggering is assumed to have been instantaneous; this may not be a bad assumption because eyewitness photographs show a rapid and dramatic onset of the blast from slide block 2. In comparing Figures 28*a* and 28*b* with the simplified model in Figure 28*c* the reader should note that only the top part of the source magma was erupted into the lateral blast. The remainder was erupted into a tall vertical eruption column during the several days after the lateral blast (see, for example, descriptions by *Lipman and Mullineaux* [1981], *Scandone and Malone* [1985], and *Carey and Sigurdsson* [1985].

Although the model can easily be scaled both geometrically and thermodynamically, one set of plausible values for initial conditions demonstrates the features of the model: an average reservoir pressure of 12.5 MPa (125 bars, the lithostatic pressure appropriate to 650 m of rock overlying the reservoir), an initial temperature of 600 K, and a mass ratio of rock to steam of 25:1. The initial temperature assumed may seem surprisingly cool if one associates volcanic eruptions only with red-hot, incandescent magma. However, many so-called "volcanic" eruptions, such as the one shown in Figure 27, are not driven by magma but by heated water ("phreatic eruptions"), or by a mixture of heated groundwater and magma ("phreatomagmatic eruptions"). The detailed nature of the volcanic gases driving the eruption is ignored here because

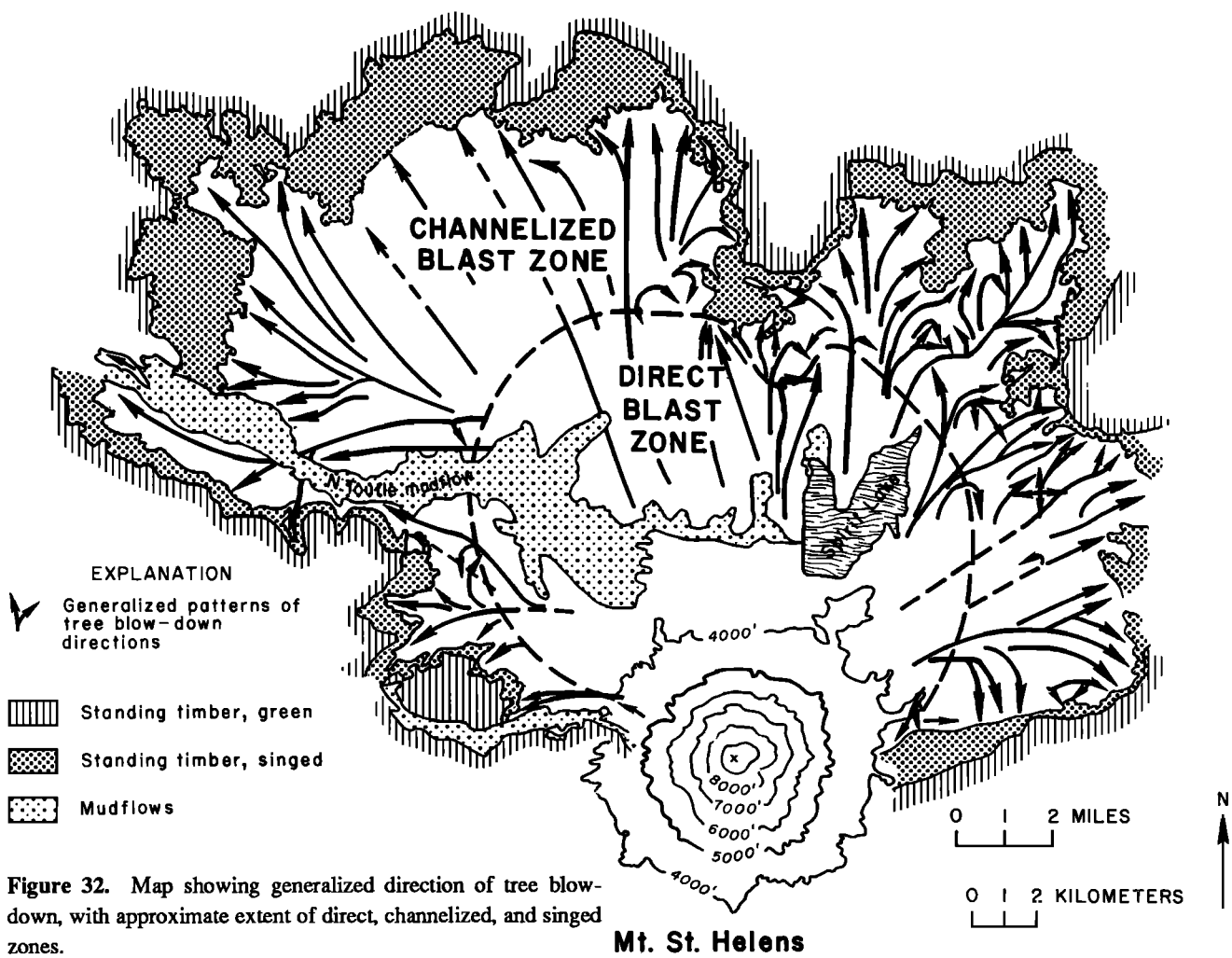

Figure 32. Map showing generalized direction of tree blowdown, with approximate extent of direct, channelized, and singed zones.

the large-scale features of the fluid mechanics are probably not sensitive to the gas source. The chosen temperature happens to be the saturation temperature of pure water at 12.5 MPa (125 bars), and it is a reasonable number to assume a priori if one believes that geothermal waters heated to saturation conditions drove the eruption (and that the badly fractured mountain edifice could not sustain any overpressure in the eruptive fluid). The temperature of 600 K can also be thought of as an average temperature for a complex mixture which, after it had traveled only a short distance, contained material ranging from the melting temperature of the magma (~1220 K) to the freezing temperature of glacial ice and snow entrained in the flow. Reasonable changes in assumed initial pressure, temperature, and solid-to-mass ratio do not qualitatively alter the conclusions. Atmospheric pressure is taken as 0.87 bar. For scale, the vent diameter is taken as 1 km, the approximate width of the scar left by the avalanches. The eruption is assumed to be centered at 2135 m elevation, and the centerline of the flow is oriented about 5° east of north to match the overall direction of the flow field. These are the only variables in the model: there are no arbitrary fitting parameters.

Nozzles operating at pressure ratios much greater than about 2:1 are supersonic. At the ratio of 125:0.87 assumed above for Mount St. Helens, the emerging flow should have been highly supersonic. The general features of supersonic flow were discussed in section 2 (Figure 2) and are shown in more detail in Figure 33*a*; the origin and significance of these features will be discussed below. In Figure 33*a*, gas is shown emerging in the axial *y* direction from a vent through plane x-x'. The gas is assumed to be a pressure higher than atmospheric and thus produces an overpressured (underexpanded) jet. Typical rarefaction waves (fans), compression waves, shock waves, and discontinuity surfaces are labeled in Figure 33*a*. Relative values of the Mach number (M) in different flow-field regions (subsonic and supersonic) are shown, and a schematic Mach disk shock is also shown. The bounding shear layer of the flow is indicated. The major features to note in this figure are the expanded shape of the jet and the existence of a complicated internal flow structure.

An enlarged view of the expansion of the flow field around the corner of a vent is shown in Figure 33*b*, which could be interpreted as a map view of the flow pattern from the east corner of the vent at Mount St. Helens. The flow at Mount St. Helens exited from a vent in the north side of the mountain; in three dimensions, therefore, the flow was not restricted by a flat surface as is implied by the way Figure 33*a* is drawn. In Figure 33*b* the stippled pattern indicates a projection of a confining surface into the plane of the flow field, but because of the three-dimensionality of the problem, the flow is free to expand beyond the half-space into which it emerges. To envision this, the

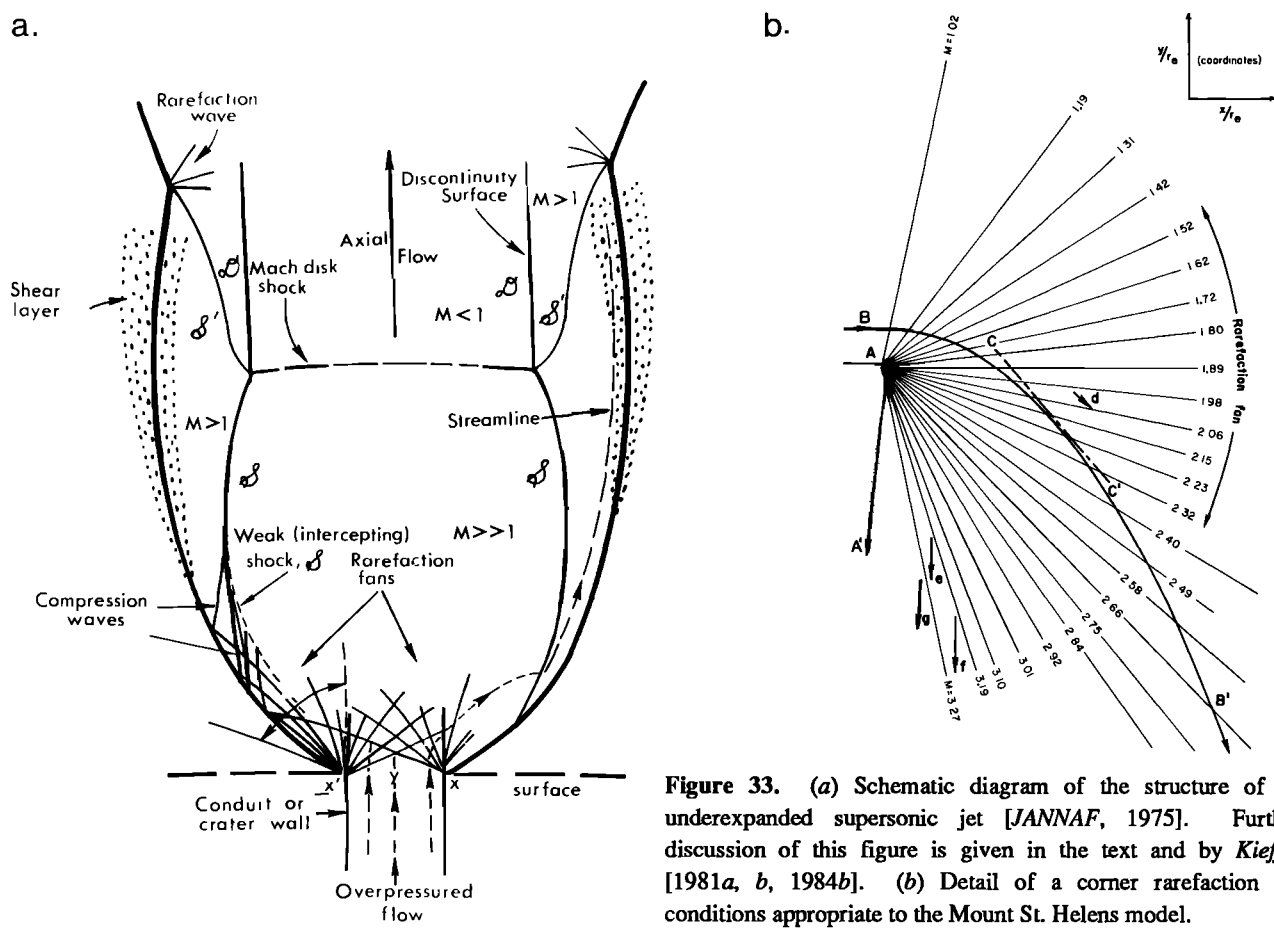

Figure 33. (*a*) Schematic diagram of the structure of an underexpanded supersonic jet [*JANNAF*, 1975]. Further discussion of this figure is given in the text and by *Kieffer* [1981*a*, *b*, 1984*b*]. (*b*) Detail of a corner rarefaction for conditions appropriate to the Mount St. Helens model.

reader might note that when gases emerge from supersonic rocket engines high in the atmosphere or in space, they can expand backward around their exhaust plane and, if the rocket is not properly designed, the exhaust gases actually can cause erosion on the sides of the rocket vehicle that they are propelling.

In Figure 33*b*, "characteristic lines" of the flow (usually just called "characteristics") are shown as the thin lines that radiate from the corner A of the vent. Characteristic lines satisfy second-order, partial differential equations of the hyperbolic type, with two independent variables [*Shapiro*, 1953]. For this analysis of Mount St. Helens the equations solved for the theoretical model are those for two-dimensional steady flow [e.g., *Thompson*, 1972, pp. 443–482]. In steady two-dimensional flow the characteristics are "Mach waves." If the characteristics are straight, the flow is termed "simple," and the characteristics are lines along which certain properties of the flow are constant. In Figure 33*b*, for example, the problem is a simple centered rarefication problem, and the Mach number M is constant on each characteristic; other physical variables can be calculated from the Mach numbers. Streamlines of the flow can be calculated from the properties of the characteristics because the turning of the flow as it crosses each characteristic is given by the method of solving the hyperbolic equations. For example, A-A′ and B-B′ are streamlines.

To relate the model to field data, I have assumed that at any point in the flow field, trees were blown down tangentially to a streamline; C-C′ is a tangent to B-B′. The small arrows d, e, f, and g represent calculated local directions of flow, as would be recorded in directions of tree blowdown. Arrows e, f, and g are particularly significant because if these are assumed to lie along flow streamlines and are extrapolated linearly backward, a flow source significantly in front of the mountain would be inferred. In compressible flow, linear extrapolations of the streamlines cannot be made because the curvature of the flow through expansion waves would not be properly accounted for.

The most important dynamic parameter of the erupting fluid is its sound speed, 105 m/s for the reservoir fluid postulated above, according to pseudogas calculations. This sound speed is about one third of the value of the atmospheric sound speed. Therefore the flow field of the volcanic pseudogas can be internally supersonic but still subsonic with respect to the surrounding atmosphere. Thus there is no contradiction between the postulated supersonic flow and the notable absence of atmospheric shock waves during the lateral blast (see eyewitness accounts in works by *Lipman and Mullineaux* [1981] and *Kieffer* [1981*a*]).

Consider first the initial velocity of the fluid. According to the proposed model, the fluid would accelerate from rest in the reservoir to sonic velocity at the vent, 100 m/s. Laboratory studies [*Kieffer and Sturtevant*, 1984] have shown that in the absence of gravitational effects the flow-front velocity of dense fluids remains at approximately the sonic velocity for many source diameters, because entrainment of the light surrounding atmosphere causes very little deceleration. At Mount St. Helens the flow would have accelerated as it dropped down the face of the mountain into the valley of the North Toutle River, but it would have declerated as it rose back up into the high country north of the Toutle River (the region now called Johnston Ridge). Because the combined effects of gravity and compressibility are not included in the model, it cannot be accurate to this level of detail. Measured velocities of the flow, averaged over substantial topographic relief to Johnston Ridge, were about 100 m/s, in good agreement with the calculated sonic velocity.

According to the model, the fluid emerged from the volcano as an underexpanded supersonic jet whose calculated flow parameters are shown in Figure 34. In Figure 34 all length dimensions are normalized to vent diameter. To ease numerical computations, the exit Mach number of the flow is assumed to have been 1.02 instead of the sonic Mach number 1.00. The boundary of flow is assumed to have been at a constant pressure of 0.87 bar and was determined from empirical formulas in *JANNAF* [1975]. The peripheral intercepting shock formed by reflection of the expansion waves from this boundary is shown as a dashed line. Because the model is symmetric about the vent axis, the plane of symmetry (centerline) acts as a rigid plane boundary, and the results can be illustrated using the two halves of the flow field to convey different information for conciseness.

On the left half of Figure 34 the characteristics are shown as light lines radiating from the corner of the vent. The characteristics here take on a much more complicated meaning than the "simple" set shown in Figure 33*b*, because throughout most of the flow field the expansion characteristics from one vent corner (shown emanating from the corner of the vent on the left) are influenced by characteristics emanating from the other vent corner (shown in the left half of Figure 34 as originating at the plane of symmetry). The fields in which the flow is "simple" in the mathematical sense are too small to show on this diagram, and throughout most of the flow field the Mach number changes continuously because of the interaction of characteristics. Therefore contours of constant properties (e.g., Mach number) must be constructed from numerical solution of the interacting characteristics. The arrows on the left side of Figure 34 represent tangents to local streamlines.

The contours of constant Mach number M are shown on the right side of Figure 34; velocities are given implicitly by the Mach numbers. By implication, these

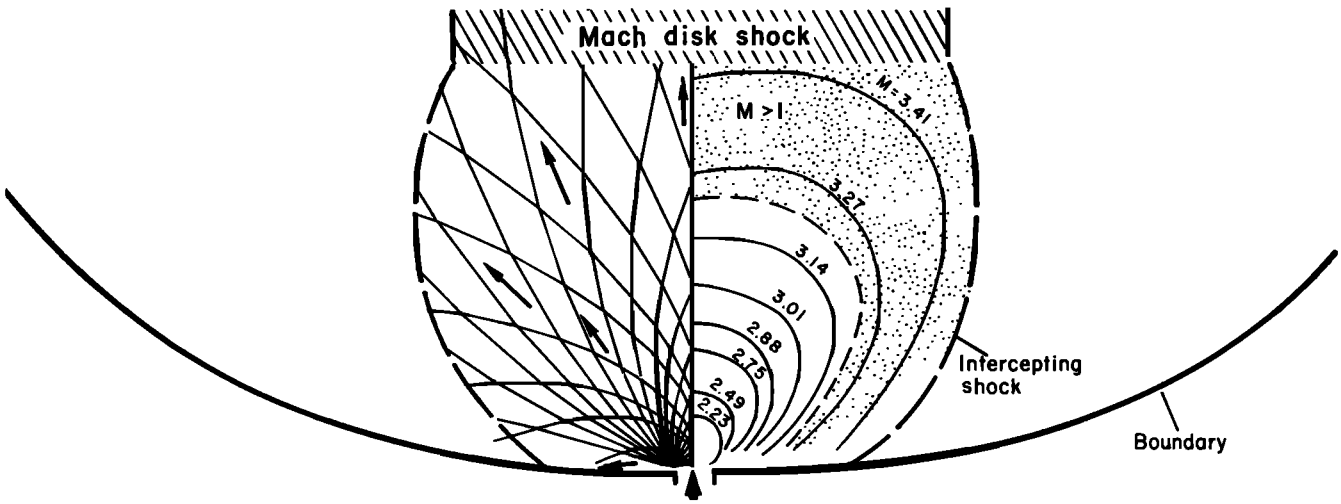

Figure 34. Map of flow field according to model of blast dynamics [*Kieffer*, 1981*a*, *b*]. (Left) Characteristics of the flow (light lines) and tangents to streamlines (vectors). (Right) Contours of nondimensional values of parameters, labeled by Mach number. From the innermost contour outward, values of M, P/P_0, T/T_0, and ρ/ρ_0 are given. In the supersonic region, these values are (2.23, 0.087, 0.91, 0.095); (2.49, 0.047, 0.89, 0.053); (2.75, 0.025, 0.87, 0.029); (2.88, 0.018, 0.86, 0.021); (3.01, 0.013, 0.85, 0.016); and (3.14, 0.009, 0.83, 0.011), respectively. See text for detailed discussion.

contours are also contours of constant pressure (P/P_0), temperature (T/T_0), and density (ρ/ρ_0). Values of these ratios are given in the figure caption.

According to the model calculations, the pressure would have decreased to 7.5 MPa (75 bars) as the fluid accelerated from the reservoir to the vent. Further decrease of the fluid pressure to ambient atmospheric pressure was accomplished through a series of complex rarefaction waves and shock waves within the jet outside the volcano, as shown schematically in Figure 33*a* and in detail in Figure 34. Because of the high pressure in the jet as it left the vent, it would have spread laterally through a characteristic angle known as the Prandtl-Meyer angle (Figure 33*b*). For the initial conditions postulated, the Prandtl-Meyer angle is 96°. Thus flow that initially was directed northward by the geometry of the vent would have diverged to the east and west. The predicted flow zone is superimposed on top of the map of the devastated area in Figure 35. I suggest that the devastated area has a southern boundary that actually curves south of an east-west line near the volcano because the initial Prandtl-Meyer expansion drove gas around in these directions.

In an underexpanded supersonic jet, rarefactions crisscross the flow and reflect off the flow boundary, assumed to be at a constant pressure equal to ambient atmospheric pressure (Figure 33*a*). Upon reflection they turn into weak compressive shocks called "intercepting" or "barrel" shocks (Figure 33*a*). The reflection of the rarefactions from the flow boundary turns the diverging flow back toward a more axial direction. I suggest that these reflections are responsible for focusing the direct blast zone so strongly to the north (Figures 32 and 35) and for limiting the extent of east-west devastation.

The fluid inside the jet expands and accelerates as it passes through the expansion waves, obtaining, according to the model, a Mach number of more than 3 on the centerline and velocities in excess of 300 m/s. Internal velocities can be locally higher than the flow-front velocity because of the internal rarefaction and shock waves. Pressure, temperature, and density decrease through the expansions. The pressure behavior is particularly interesting and illustrates the nonlinearity of the supersonic expansion process: as the fluid expands, the pressure decreases below atmospheric pressure, and a large zone of subatmospheric pressure develops inside the supersonic zone (see the shaded area in Figures 34 and 35). The numerical model discussed by *Kieffer* [1984*b*, p. 155] suggests that the pressure in this region could be as low as 4% of atmospheric pressure. The existence of such a low-pressure core has some interesting volcanic hazards implications: for example, plastic components on vehicles in or near this part of the devastated area were degraded by the formation of large vapor bubbles [*Davis and Graeber*, 1980]. Laboratory studies demonstrated that the vapor formation was caused by exposure of the plastic to high temperatures during the blast. Efforts to duplicate the degradation by heating similar plastics in the laboratory under atmospheric pressure produced general similarities but failed to produce the large size of the bubbles found on the components from the vehicles. I speculate that bubbles may have grown unexpectedly large because the external pressure was temporarily lower than atmospheric in the supersonic core of the lateral blast.

In an underexpanded jet the intercepting shocks strengthen within the flow and coalesce across it into a strong shock standing perpendicular to the axis of the flow.

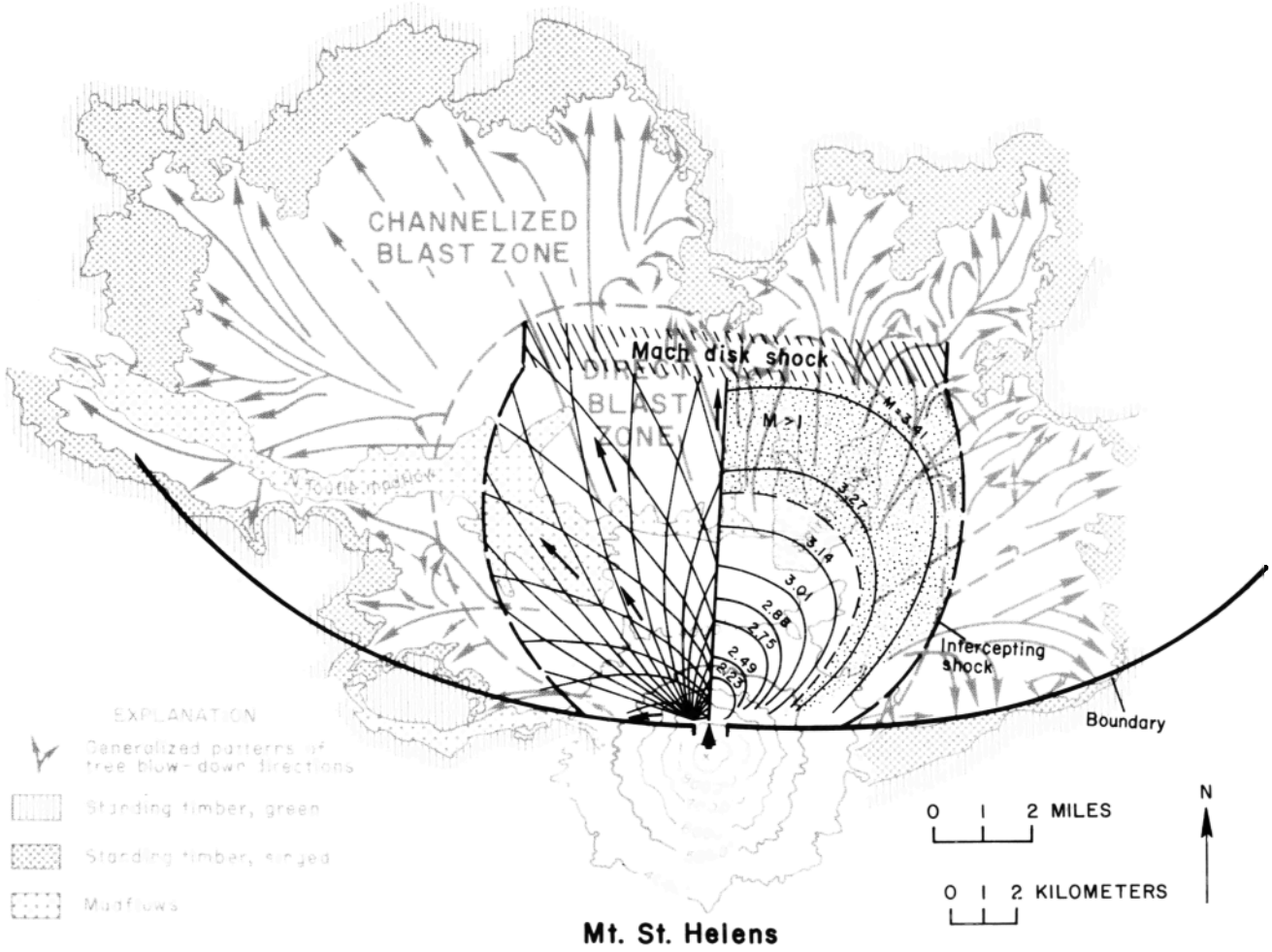

Figure 35. The model of Figure 34 superimposed on the map of the devastated area. The coincidence of the Mach disk with the direct blast zone boundary in the northerly direction suggested to the author that the direct blast zone was a zone of strong supersonic flow.

This shock is called the "Mach disk" (Figure 33*a*). As gas flows through the shock, it decelerates from supersonic to subsonic conditions; to a first approximation, the pressure on the downstream side of the Mach disk is atmospheric. Inertia of the heavy debris entrained by the blast at the Mach disk (the overturned logging vehicle in Figure 30*a* and the debris around it give some impression of the size of the debris load near the Mach disk) would propel the particulate matter through a "gas shock," so that the Mach disk should, in this geologic case, be thought of as a Mach disk "zone," perhaps of the order of 1 km in thickness. As the fluid decelerates into the subsonic zone downstream of the Mach disk, flow velocities decrease, pressure rises from subatmospheric back toward atmospheric, and the density of the fluid increases. According to the calculations, the Mach disk would have stood about 11 km north of the vent. The calculated position and, to a lesser extent, the position of the lateral intercepting shocks coincide roughly with the boundaries between the direct and channelized blast zones (Figure 35). I propose that these two zones correspond roughly to the boundary between supersonic and subsonic flow regimes within the lateral blast.

A computer model that produced a somewhat smaller supersonic zone because the flow boundary was assumed to be inviscid rather than viscous (as in the above model) was run for the author by R. A. O'Leary (Rocketdyne) [*Kieffer*, 1984*b*]. Differences between the two models are not significant in terms of our lack of knowledge of the real complexities of the eruption, e.g., material emerging from two moving landslides instead of from a single vertical vent. No existing model is adequate for calculating properties beyond the Mach disk shock (compare discussions by *Kieffer* [1981*a*, 1984*b*]). I believe that the most plausible assumption is that the flow is returned to ambient atmospheric pressure beyond the Mach disk (and perhaps beyond the peripheral intercepting shocks) and that compressibility plays a much less important role in the flow field beyond these features.

Because of the dramatic deceleration of the flow at the Mach disk, gravity (which was not a dominant force within the direct blast zone) dominated flow mechanics outside of this zone, that is, in the channelized blast zone. Thus the flow streamlines, as indicated by the tree blowdown patterns, are more influenced by topography in the channelized, subsonic zone. The devastated area therefore

consists of two parts: the inner direct blast zone, in which gas dynamics effects and supersonic flow were probably dominant, and the surrounding channelized blast zone, in which downhill flow driven by gravity was probably dominant. This is an oversimplification, because both effects were probably important throughout much of the devastated area (for example, the most highly supersonic zone and the Mach disk happen to coincide with a region of very steep topography), and quantitative modeling including both effects is required in the future.

Temperatures throughout a particle-laden flow like the lateral blast are remarkably high and uniform because of the high mass ratio of solids to vapor (this is the effect of $\gamma \sim 1$; see Figure 4 and equation (2)). Calculated temperatures changed only from 600 K to 480 K at the limits of the devastated area; these temperatures are in excellent agreement with temperatures measured in the deposits immediately after the eruption (see articles in the work by *Lipman and Mullineaux* [1981]).

Several other properties of the blast can be calculated from this model. For example, the maximum mass flux is calculated to have been 10^4 g s^{-1} cm^{-2}, and the thermal flux to have been 2.5 MW/cm^2. The calculated total energy of the blast was 24 megatons (Mt), of which 7 Mt was dissipated during the blast itself, and the remaining 17 Mt was dissipated during the almost simultaneous condensation of steam in the blast and the subsequent cooling of steam and rock to ambient temperature in the weeks following May 18.

As mentioned above, the supersonic flow model for the lateral blast has been controversial. Nevertheless, features analogous to those eroded into the surfaces of supersonic reentry vehicles have been found in the erosion surface under the blast deposits [*Kieffer and Sturtevant*, 1988].

7. PERSPECTIVES

In the discussions of Crystal Rapids and Old Faithful Geyser, I have pointed out specific directions for future research. At Mount St. Helens, unequivocal re-creation of the fluid dynamics of the lateral blast may be difficult in spite of the fact that it is the best documented violent volcanic eruption in recorded history. The observational problems inherent in geologic research, and particularly in the monitoring of geologically rare events, are enormous. Nevertheless, the evolution of fluid dynamics in geology over the past few decades has been rapid, namely, the pioneering work of Wilson and his colleagues and students (reviews are given by *Wilson and Head* [1983] and *Sparks*, [1983]).

It is appropriate to conclude with the thought that the development of modern spacecraft, which is responsible for much of the theory of compressible gas dynamics on which this paper is based, has led to one of the most exciting discoveries of modern times—the existence of erupting volcanoes on another planet, Io (see the summary by *Morrison* [1982] and the interpretation by *Kieffer* [1982]). Because of the large ratios of conduit and vent pressure to atmospheric pressure on Io (and perhaps in past volcanism on Mars and the Moon), geologists and planetary scientists will continue to pose problems of scale, chemical complexity, and geometry that will present challenging fluid dynamics problems for decades to come.

ACKNOWLEDGMENTS. This paper is dedicated to Hans W. Liepmann, a pioneer in fluid dynamics, on the occasion of his seventieth birthday. The studies described here have extended over 12 years and have involved many colleagues to whom I owe thanks, including those referenced or mentioned as "private communication" in this article, and numerous others who could not be referenced because of space limitations: colleagues who work within the National Science Foundation, the U.S. Geological Survey, and the Bureau of Reclamation to help fund the work; and, Eugene Shoemaker and Bradford Sturtevant who interested me in, and taught me, fluid dynamics as a student from the text by Liepmann and Roshko. Finally, special thanks are owed to a supportive husband, who has encouraged all of my work, and to our son—a valuable field assistant.

The editors for this paper were W. R. Peltier and M. Neugebauer. They thank an anonymous referee for his assistance in evaluating the technical content of this paper and P. L. Richardson for serving as a cross-disciplinary referee.

REFERENCES

Biasi, L., A. Prosperetti, and A. Tozzi, Collapse of a condensing bubble in compressible liquids, *Chem. Eng. Sci., 72*, 815–822, 1972.

Birch, F., and G. C. Kennedy, Notes on geyser temperatures in Iceland and Yellowstone National Park, in *Flow and Fracture of Rocks, Geophys. Monogr. Ser.* vol. 16, edited by H. C. Heard et al., pp. 329–336, 1972.

Carey, S., and H. Sigurdsson, The May 18, 1980 eruption of Mount St. Helens, 2, Modeling of dynamics of the Plinian phase, *J. Geophys. Res., 90*, 2948–2958, 1985.

Chen, C. J., and W. Rodi, *Vertical Turbulent Buoyant Jets—A Review of Experimental Data*, 83 pp., Pergamon, New York, 1980.

Davis, M. J., and E. J. Graeber, Temperature estimates of May 18 eruption of Mount St. Helens made from observations of material response (abstract), *Eos Trans. AGU, 61*, 1136, 1980.

Eichelberger, J. C., and D. B. Hayes, Magmatic model for the Mount St. Helens blast of May 18, 1980, *J. Geophys. Res., 87*, 7727–7738, 1982.

Fauske, H. K., Contribution to the theory of two-phase, one-component critical flow, *Argonne Natl. Lab. Rep. ANL 6633*, 1962.

Fujikawa, S., and T. Akamatsu, Experimental investigations of cavitation bubble collapse by a water shock tube, *Bull. Jpn. Soc. Min. Eng., 21*, 223–230, 1978.

Fujikawa, S., and T. Akamatsu, Discussion and reply, *Bull. Jpn. Soc. Min. Eng., 22*, 279–281, 1979.

Fuller, S., and J. Schmidt, *Yellowstone in Three Seasons*, 48 pp., Snow Country Publications, Yellowstone National Park, Wyo., 1984.

Hentschel, W., Akustische und optische Untersuchungen zur Dynamik holografisch erzeugter Kavitations-blasen-Systeme, Master's thesis, Göttingen Univ., 1979.

Hentschel, W., Zur Dynamik Laserzeugter Kavitationblasen, *Fortschr. Akustik, DAGA '80*, 415–418, 1980.

Hjülstrom, F., Studies of the morphological activity of rivers as illustrated by the river Fyris, *Univ. Uppsala Geol. Inst. Bull., 25*, 221–527, 1935.

JANNAF (Joint Army, Navy, NASA, Air Force), Handbook of rocket exhaust plume technology, *Publ. 263*, chap. 2, 237 pp., Chemical Propulsion Information Agency, Johns Hopkins Univ. Appl. Phys. Lab., Laurel, Md., 1975.

Kieffer, S. W., Sound speed in liquid-gas mixtures: Water-air and water stream, *J. Geophys. Res., 82*, 2895–2904, 1977.

Kieffer, S. W., Fluid dynamics of the May 18 blast at Mount St. Helens, *U.S. Geol. Surv. Prof. Pap., 1250*, 379–400, 1981*a*.

Kieffer, S. W., Blast dynamics at Mount St. Helens on 18 May 1980, *Nature, 291*, 568–570, 1981*b*.

Kieffer, S. W., Dynamics and thermodynamics of volcanic eruptions: Implications for the plumes on Io, in *Satellites of Jupiter*, edited by D. Morrison, pp. 647–723, University of Arizona Press,Tucson, 1982.

Kieffer, S. W., Seismicity at Old Faithful Geyser: An isolated source of geothermal noise and possible analogue of volcanic seismicity, *J. Volcanol. Geotherm. Res., 22*, 59–95, 1984*a*.

Kieffer, S. W., Factors governing the structure of volcanic jets, in *Explosive Volcanism: Inception, Evolution, and Hazards*, edited by F. M. Boyd, chap. 11, pp. 143–157, National Academy Press, Washington, D.C., 1984*b*.

Kieffer, S. W., The 1983 hydraulic jump in Crystal Rapid: Implications for river-running and geomorphic evolution in the Grand Canyon, *J. Geol., 93*, 385–406, 1985.

Kieffer, S. W., Hydraulic maps of major rapids of the Colorado River, Grand Canyon, Arizona, *U.S. Geol. Surv. Misc. Invest. Maps, 1897 A-J*, 1988.

Kieffer, S. W., and J. Delany, Isentropic decompression of fluids from crustal and mantle pressures, *J. Geophys. Res., 84*, 1611–1620, 1979.

Kieffer, S. W., and B. Sturtevant, Laboratory studies of volcanic jets, *J. Geophys. Res., 89*, 8253–8268, 1984.

Kieffer, S. W., and B. Sturtevant, Erosional furrows formed during the lateral blast at Mount St. Helens, May 18, 1980, *J. Geophys. Res., 93*, 14,793–14,816, 1988.

Kieffer, S. W., and J. Westphal, Pressure and temperature measurements in Old Faithful Geysers, *Eos Trans. AGU, 66*(46), 1152, 1985.

Leet, R. C., Saturated and subcooled hydrothermal boiling in groundwater flow channels as a source of harmonic tremor, *J. Geophys. Res., 93*, 4835–4849, 1988.

Liepmann, H. W., and A. Roshko, *Elements of Gasdynamics*, 439 pp., John Wiley, New York, 1957.

Lipman, P. W., and D. R. Mullineaux (Eds.), The 1980 Eruptions of Mount St. Helens, Washington, *U.S. Geol. Surv. Prof. Pap., 1250*, 844 pp., 1981.

Loh, W. H. T. (Ed.), *Modern Developments in Gas Dynamics*, 386 pp., Plenum, New York, 1969.

Malin, M., and M. Sheridan, Computer-assisted mapping of pyroclastic surges, *Science, 217*, 637–640, 1982.

McKee, C. O., D. A. Wallace, R. A. Almond, and B. Talais, Fatal hydro-eruption of Karkar volcano in 1979: Development of a maar-like crater, in *Cooke-Ravian Volume of Volcanological Papers*, edited by R. W. Johnson, *Geol. Surv. Papua New Guinea Mem., 10*, 63–84, 1981.

Moody, F. J., Maximum flow rate of a single component two phase mixture, *J. Heat Transfer, 87*, 134–142, 1965.

Moore, J. G., and W. C. Albee, Topographic and structural changes, March–July 1980—Photogrammetric data, in *The 1980 Eruptions of Mount St. Helens, Washington, U.S. Geol. Surv. Prof. Pap. 1250*, edited by P. W. Lipman and D. R. Mullineaux, pp. 123–134, 1981.

Moore, J. G., and C. Rice, Chronology and character of the May 18, 1980, explosive eruptions of Mount St. Helens, in *Explosive Volcanism: Inception, Evolution, and Hazards*, edited by F. M. Boyd, chap. 10, pp. 133–157, National Academy Press, Washington, D. C., 1984.

Morrison, D., *Satellites of Jupiter*, 972 pp., University of Arizona Press, Tucson, 1982.

Riabouchinsky, D., Mécanique des fluides, *C. R. Acad. Sci., 195*, 998–999, 1932.

Richards, K., *Rivers: Form and process in Alluvial Channels*, p. 58, Methuen, London, 1983.

Scandone, R., and S. Malone, Magma supply, magma discharge, and readjustment of the feeding system of St. Helens during 1980, *J. Volcanol. Geotherm. Res., 23*, 239–262, 1985.

Shapiro, A. H., *The Dynamics and Thermodynamics of Compressible Fluid Flow*, vol. 1, 647 pp., John Wiley, New York, 1953.

Sparks, R. S. J., Fluid dynamics in volcanology, *J. Volcanol., 46*(4), 325–331, 1983.

Thompson, P. A., *Compressible-Fluid Dynamics*, pp. 517–531, McGraw-Hill, New York, 1972.

Turner, J. S., Jets and plumes with negative or reversing buoyancy, *J. Fluid Mech., 26*, 779–792, 1966.

Wallis, G. B., *One-Dimensional, Two-Phase Flow*, 408 pp., McGraw-Hill, New York, 1969.

White, D. E., Some principles of geyser activity mainly from Steamboat Springs, Nevada, *Am. J. Sci., 265*, 641–684, 1967.

Williams, S. N., and H. Meyer, A model of Nevado del Ruiz Volcano, Colombia, *Eos Trans. AGU, 69*, 1554, 1988.

Wilson, L., and J. W. Head III, A comparison of volcanic eruption processes on Earth, Moon, Mars, Io, and Venus, *Nature, 302*, 663–669, 1983.

Zucrow, M. G., and J. D. Hoffman, *Gas Dynamics*, vol. 1, 772 pp., vol. 2, 480 pp., John Wiley, New York, 1976.

S. W. Kieffer, U.S. Geological Survey, Branch of Igneous and Geothermal Processes, 2255 North Gemini Drive, Flagstaff, AZ 86001.